Arthritis & Rheumatology
Vol. 0, No. 0, Month 2026, pp 1–19
DOI 10.1002/art.70047

American College of Rheumatology
Empowering Rheumatology Professionals

Dual Action of Dipyridamole in Experimental Rheumatoid Arthritis: Suppression of Joint Inflammation and Upregulation of Muscle Anabolism via Adenosine and AMPK Pathways

Miguel Marco-Bonilla, MSc,[1] Maria Fresnadillo, MSc,[1] Irene Sanchez-Platero, MSc,[1] Macarena de la Riva-Bueno, MSc,[1] Fernando Huete-Toral, PhD,[2] Gonzalo Carracedo, PhD,[2,3] Carmen Conde, PhD,[4] Yolanda Benitez, MSc,[5] Pablo Minguez, PhD,[5,6,7] Sandra Carolina Cifuentes, PhD,[8] Joaquin Rams, PhD,[8] Gabriel Herrero-Beaumont, MD, PhD,[1] Raquel Largo, PhD,[1] and Aránzazu Mediero, PhD[1]

Objective. Rheumatoid sarcopenia, characterized by the progressive loss of skeletal muscle mass and function, is a frequent comorbidity in rheumatoid arthritis (RA), linked to prolonged, severe systemic inflammation. Purinergic signaling (adenosine, AMP, and ATP) plays a crucial role in inflammation, myogenesis, and muscle hypertrophy. Dipyridamole, an antiplatelet agent, enhances extracellular adenosine availability, alters AMP/ATP ratio, and activates A2BR and AMP kinase (AMPK) pathways. We aim to investigate its potential use as a therapeutic agent for RA and rheumatoid sarcopenia.

Methods. K/BxN-induced mice received preventive or therapeutic dipyridamole treatment daily and were sacrificed at joint inflammation peak and resolution stage. Motor activity tests and dual-energy x-ray absorptiometry were performed. C-reactive protein levels were also analyzed in serum, and cytokines array was performed in serum and muscle. Histology of tibialis anterior and talus joint were studied. Myogenesis, purinergic system, atrophy, and senescence key markers were analyzed via Western blot and reverse transcriptase–polymerase chain reaction in gastrocnemius. Nucleotide content via high-performance liquid chromatography was performed. Two-dimensional and three-dimensional models with C2C12 cells were done.

Results. Dipyridamole reduced joint, muscle, and systemic inflammation, counteracting muscle wasting and physical inactivity via an anabolic mechanism involving down-regulation of myostatin expression. This effect was mediated by increased adenosine and AMP levels, which activate adenosine A2BR and downstream cAMP/AMPK signaling pathways.

Conclusion. These results support a dual role for dipyridamole in RA, combining robust anti-inflammatory effects with a novel, myostatin-linked anabolic action on sarcopenia, mediated through adenosine and AMPK signaling, distinct from conventional therapeutic mechanisms.

INTRODUCTION

Rheumatoid arthritis (RA) is a chronic autoimmune disease characterized by inflammation of the joints. Although this is the main feature, RA can affect others tissues due to the elevated chronic systemic inflammation.[1] RA can lead to alterations in body composition, including a reduction in muscle mass (lean mass) and either stable or increased fat mass, changes that may

Supported by the Instituto de Salud Carlos III (ISCIII; grants PI22/00347 and PI22/00352), European Union, and Health Outcomes-Oriented Cooperative Research Networks (grants RD21/0002/0025 and RD24/0007/0031), granted by the ISCIII and funded by the European Union—NextGenerationEU via Mecanismo de Recuperación, Transformación y Resiliencia.

[1]Joint and Bone Research Unit, Fundación Instituto de Investigación Sanitaria de la Fundación Jiménez Díaz, Universidad Autónoma de Madrid, Madrid, Spain; [2]Ocupharm Group Research, Faculty of Optic and Optometry, University Complutense of Madrid, Madrid, Spain; [3]Department of Optometry and Vision, Faculty of Optic and Optometry, University Complutense of Madrid, Madrid, Spain; [4]Laboratorio de Reumatología Experimental y Observacional, Instituto de Investigación Sanitaria de Santiago, Hospital Clínico Universitario de Santiago de Compostela, Servicio Gallego de Salud, Santiago de Compostela, Spain; [5]Bioinformatics Unit, Fundación Instituto de Investigación Sanitaria de la Fundación Jiménez Díaz, Universidad Autónoma de Madrid, Madrid, Spain; [6]Department of Genetics, Fundación Instituto de Investigación Sanitaria de la Fundación Jiménez Díaz, Universidad Autónoma de Madrid, Madrid, Spain; [7]Center for Biomedical Network Research on Rare Diseases, Instituto de Salud Carlos III, Madrid, Spain; [8]Department of Applied Mathematics, Materials Science and Engineering and Electronic Technology, Universidad Rey Juan Carlos, Mostoles, Spain.

Mr Marco-Bonilla and Ms Fresnadillo are co-first authors and contributed equally to this.

Additional supplementary information cited in this article can be found online in the Supporting Information section (https://acrjournals.onlinelibrary.wiley.com/doi/10.1002/art.70047).

not be reflected in body mass index.[1] Muscle atrophy is already present before pain and swelling affect the physical activity of patients with RA, indicating that muscle is affected from the earliest stages of RA.[1] Secondary sarcopenia, which refers to muscle loss and a decline in physical activity resulting from disease, malnutrition, or physical disability, contrasts with primary sarcopenia, a multifactorial condition associated with aging.[1] Studies in the literature report that the prevalence of rheumatoid sarcopenia ranges from 20% to 44%, an interval that is justified, among other reasons, by the lack of universally accepted clinical criteria for its diagnosis.[1]

Muscle homeostasis is preserved through an accurate balance between anabolic and catabolic processes.[1] Previous data in rabbit experimental RA antigen-induced arthritis (AiA) showed that increased inflammation produces muscle loss by the increase of atrogenes that produces muscle atrophy.[2] The high production of the inflammatory cytokines, like tumor necrosis factor-α (TNF-α), interleukin-1β (IL-1β), IL-6, or interferon-γ (IFN-γ), work synergistically to promote rheumatoid sarcopenia by shifting protein metabolism toward net catabolism, elevating muscle proteolysis, disruption of muscle satellite cells self-renewal, direct impairment of myofiber force, muscle atrophy, and fibrosis.[3,4] Unfortunately, methotrexate (MTX), one of the most commonly used conventional synthetic disease-modifying antirheumatic drugs (DMARDs), has shown no beneficial effects on muscle tissue in animal models of RA.[5] Similarly, treatments with MTX and biologic DMARDs (bDMARDs), although effective in achieving RA remission, do not appear to improve muscle condition in patients.[6] This persistent musculoskeletal disorder suggests a "permanent imprint" that remains even after effective control of inflammation.[7] Therefore, DMARDs and biologic therapies may not be sufficient to counteract muscle loss in RA.[6]

The purinergic system, which involves nucleosides and nucleotides, such as adenosine and ATP, regulates the inflammatory response.[8–10] Overall, adenosine signaling through adenosine receptors constitutes a critical interface between extracellular signaling and intracellular cAMP pathway or AMP kinase (AMPK) activation.[9] In particular, adenosine receptors A2AR and A2BR play a protective role by activating anti-inflammatory pathways, as supported by previous findings.[11,12] In addition, A2BR is essential for muscle homeostasis maintenance. Stimulation with agonists increases muscle weight and activity in high-fat diet mice, suggesting an anabolic effect in muscle via this receptor.[10] Also, the use of A2BR agonist on mice with age-related sarcopenia enhances muscle strength and muscle-specific A2BR knockout led to reduced muscle mass and strength. In humans, A2BR expression in muscle has a negative correlation with aging.[10] These findings suggest that A2BR activation may represent a promising target to prevent or reverse muscle atrophy associated with aging or chronic diseases.

The purinergic system can be modulated using pharmacological agents that modify adenosine and ATP levels.[13] In fact, the anti-inflammatory effect of MTX in human RA may be explained by this mechanism of action.[14] Dipyridamole, an antiplatelet drug that inhibits phosphodiesterase 3, blocks nucleoside transport via ENT1/2/4, thereby increasing extracellular adenosine concentrations by preventing cellular uptake.[15] This accumulation of extracellular adenosine leads to the sustained activation of adenosine receptors, particularly A2AR and A2BR.[9,13] Preliminary data suggested that dipyridamole could promote an anti-inflammatory effect in experimental RA.[16] Beyond this anti-inflammatory role of dipyridamole, our previous research demonstrated that this drug exerts a direct effect on muscle cells, preventing disruptions in myogenesis by increasing extracellular adenosine level, leading to A2BR activation.[9] Additionally, dipyridamole elevated both cAMP and intracellular AMP levels, thereby facilitating AMPK activation and preventing myogenic alterations.[9]

However, the specific interaction between the purinergic system and rheumatoid sarcopenia remains unexplored. Therefore, our aim was to determine the therapeutic potential of dipyridamole in RA and rheumatoid sarcopenia and to evaluate the role of adenosine and purinergic signaling in mediating muscle pathology.

MATERIALS AND METHODS

All the reagents and resources used are defined in Supplementary Table S1. The raw and processed RNA-sequencing data generated in this study have been deposited in NCBI's GEO and are accessible through GEO Series accession number GSE274162. All remaining data are available on reasonable request. Patients were not involved in this research.

K/BxN serum transfer–induced arthritic model. Animal management and experimentation complied with the Spanish Regulations and the European Union Guidelines for the Care and Use of Laboratory Animals and were approved by the Institutional Ethics and Welfare Committee of the Jiménez Díaz Foundation University Hospital and Research Institute (PROEX 19/019 and PROEX 019.6/24).

K/BxN mice were generated by crossing KRN mice with NOD/Lt mice. Serum was collected from adult arthritic K/BxN mice and pooled for use in experiments. Twelve-week-old, age-matched male C57BL/6J mice were obtained from Charles River Laboratories (Barcelona, Spain) and randomly assigned to five experimental groups employing research-randomizer free

Author disclosures and graphical abstract are available at https://onlinelibrary.wiley.com/doi/10.1002/art.70047

Address correspondence via email to Aránzazu Mediero, PhD, at aranzazu.mediero@iis-fjd.es.

Submitted for publication June 25, 2025; accepted in revised form December 15, 2025.

software: (1) Sham (healthy): no serum transfer (N = 8); (2) Dipy (healthy + dipyridamole): healthy mice treated with dipyridamole at 25 mg/kg/day, administered daily starting on day 0 (N = 5); (3) RA (arthritic control [Ctrl]): mice received 100 μL of pooled serum via intraperitoneal (IP) injection on days zero and two to induce arthritis (N = 7–8); (4) RA + Dipy D0: arthritic mice treated with dipyridamole at 25 mg/kg/day, administered daily starting on day zero, along with serum transfer (100 μL IP on days 0 and 2; preventive treatment; N = 6–7); or (5) RA + Dipy D7: arthritic mice treated with dipyridamole at 25 mg/kg/day, administered daily starting on day seven, with serum transfer as above (therapeutic treatment; N = 7–8).

To evaluate the ability of adenosine A2AR or A2BR antagonist to inhibit the effect of dipyridamole both in inflammation and development of sarcopenia, the following experimental groups were repeated and included: (1) RA (N = 3); (2) RA + Dipy D0 (N = 3); (3) RA + A2AR antagonist + Dipy D0: arthritic mice treated with the A2AR antagonist SCH58261 (1 mg/kg/day) and dipyridamole (25 mg/kg/day), both administered daily starting on day zero, together with serum transfer (100 μl IP on days 0 and 2; N = 5); and (4) RA + A2BR antagonist+ Dipy D0: arthritic mice treated with the A2BR antagonist PSB603 (1 mg/kg/day) and dipyridamole (25 mg/kg/day), both administered daily starting on day zero, together with serum transfer (100 μl IP on days 0 and 2; N = 5).

Animals with RA were identified using ear tags to avoid confounders. The same three experimental investigators were responsible for animal allocation at all stages.

RA progression was evaluated daily, and the severity of RA in each paw was assessed using a four-point scale: zero for healthy appearance, one for edema and erythema in one surface of the paw, two for edema and erythema including more than one surface of the paw, and three to four for edema and erythema in whole paw. The scores from all four paws were summed up to create a combined score. Mice were weighed weekly. All motor activity tests were performed before serum inoculation and before sacrifice. Mice were sacrificed at two different times: on day 15 (highest point of macroscopic inflammation) and on day 28 (not macroscopic inflammation detected in the joints; resolution stage) after serum injection. Representative images of body structure and paw's muscles were taken on sacrifice days. Gastrocnemius (GA) was collected for protein and RNA extraction, nucleotide analysis via high-performance liquid chromatography (HPLC), and measurement of cytokines and chemokines. Tibialis anterior (TA) was included in OCT for freeze histology. Talus joints were decalcified in 10% EDTA and paraffin embedded for histology. Blood was drawn, and serum was isolated for measurement of C-reactive protein (CRP) and cytokines.

Ambulatory activity. For ambulatory activity, mice were placed in separate recording chambers and given six minutes to freely move. Distance traveled by each mouse was tracked using Kinovea open-source video analysis software. Data were represented as the difference between the highest point of inflammation or resolution stage and the baseline.

Two-limb hanging test. The test was performed maintaining the parameters established by Aartsma-Rus and van Putten.[17] Data were represented as in the ambulatory activity section described.

Forelimb grip strength test. The Grip Strength Meter was used to assess the grip strength peak of the forelimbs. Grip measurements were repeated three times and kept the average grip value. Data were represented as in the ambulatory activity section described.

Rotarod. The synchronized motor ability of all four limbs was evaluated using a rotarod test. Initially, mice were introduced to the rotarod by allowing them to spend 120 seconds on the rod, which rotated at speeds of 4 and 6 rotations per minute. Motor function was evaluated by familiarizing the mice with an accelerated rotarod procedure comprising three trials. During these trials, the rod accelerated from 4 rpm to 40 rpm within five minutes. Each trial had a maximum duration of 300 seconds and ended either when the mouse fell or ceased walking on the rotating rod. The data shown were analyzed before sacrifice and did not correlate with baseline values because activity learning was conducted once a week before testing.

Dual-energy x-ray absorptiometry. Before RA induction and sacrifice day, all mice underwent dual-energy x-ray absorptiometry (DXA) scan using a Lunar PIXImus densitometer (Lunar, Madison, WI). The scan was calibrated before each scanning session using a hydroxyapatite phantom with known bone mineral density (BMD) supplied by the manufacturer. Afterward, mice were anesthetized by ketamine and xylazine and placed in the prone position for complete body scans. The analysis involved examining whole-body lean mass, fat mass, BMD, and bone mineral content (BMC). Data are presented as the change from baseline to the resolution stage.

Quantification of serum CRP. Serum CRP was determined by Mouse CRP ELISA Kit, according to manufacturer instructions. Absorbance was measured at 450 nm using a microplate reader.

Cytokines and chemokines array. The effect of dipyridamole on the concentration of several cytokines both systemically and locally was assessed using Mouse Cytokine Array Q1, kit which simultaneously detects 20 cytokines. The cytokines concentration was measured by fluorescence using GenePix 4000B following manufacturer protocol for serum and frozen GA. Serum samples were used at two-fold sample dilution.

Frozen GA was crushed using a mortar and a pestle cooled with liquid nitrogen and was homogenized in a sonicator, and the protein isolated in the supernatant was quantified with bicinchoninic acid (BCA) assay. A total of 100 μl (1 mg/mL) of GA protein was used.

Talus joint histology. The 5-μm sections underwent hematoxylin and eosin (H&E) staining. Representative images were taken with optical microscope of talus and tibia bones space (20× magnitudes) or talus synovial tissue (4×). Quantification of synovitis histologic features (Krenn score) was performed as previously reported.[18] One animal from the Dipy group was excluded from analysis because the integrity of the synovial tissue had not been preserved in earlier steps.

Histologic analysis of TA. The 10-μm sections were brought from –80°C to room temperature and immediately immersed in methanol for 30 minutes to improve fixation and stained with H&E. Images were taken with optical microscope (20× magnification). Analysis of cross-sectional area (CSA) in five representative images was performed with ImageJ using the Muscle Morphometry plugin.

For ATPase staining, 10-μm cross-sections were immersed for 45 minutes in a solution containing 0.1 M glycine/NaCl buffer with pH 9.4, along with 0.75 M $CaCl_2$ and 5 mg ATP. Following a rinse in distilled water, the sections were placed in 2% cobalt chloride solution and subsequently treated with diluted (1/10) ammonium chloride to reveal type I (white) and type II (black) fibers. Finally, the sections were dehydrated and mounted using dibutylphthalate polystyrene xylene (DPX) mounting medium. Fiber type quantification of five representative images taken with optical microscope (20× magnification) was performed using the ImageJ software.

Picrosirius Red staining was performed to visualize tissue fibrosis. The 10-μm sections were air-dried for 30 minutes at room temperature and fixed in paraformaldehyde (PFA) 4% for 30 minutes. Next, sections were incubated for 90 minutes in 0.1% Sirius Red solution dissolved in aqueous saturated picric acid and immersed immediately in 0.1 M HCl solution for 1 minute. Sections were washed two times in H_2O, dehydrated, and mounted with DPX. Five representative pictures were taken with bright field and polarized light in an optical microscope (×20 magnification). Quantification of collagen I was performed using the ImageJ software on polarized images.

For necrosis measurement, 10-μM sections were air-dried and fixed in PFA 4% for 20 minutes. Sections were washed three times for five minutes and blocked with 5% bovine serum albumin (BSA) in phosphate-buffered saline (PBS) for one hour. Then, sections were incubated overnight with laminin antibody in a humid chamber. After three washes, sections were incubated with Alexa Fluor 594 red-fluorescent secondary antibody to rabbit IgG and Alexa Fluor 488 green-fluorescent secondary antibody to mouse IgG. IgG immunoreactivity within myofibers indicates myonecrosis in TA. Five representative pictures were taken with a fluorescence microscope (×20 magnification) in random chosen fields for each labeling. Analysis with Fiji was performed to study the percentage of positive IgG-stained fibers per field of view.

cAMP and creatine measurements. cAMP and creatine concentration were quantified in 50 μg of crushed GA using colorimetric assays following manufacturer's recommendations. Colorimetric reaction was measured at 450 nm for cAMP or 570 nm for creatine in a microplate reader (Tecan Spark 20M).

RNA sequencing and bioinformatic analysis. RNA was isolated from GA (20μg) of RA and RA + Dipy D0 groups on day 15 after serum induction (n = 4 each) following the RNeasy Fibrous Tissue Mini Kit. Library preparation and sequencing were conducted in Fundación Parque Científico de Madrid. Total RNA quality and concentration was assessed on 4200 TapeStation, using an RNA ScreenTape. Then, 500 ng of total RNA from each sample were used as input for library preparation with NEBNext Ultra II Directional RNA Library Prep Kit for Illumina, following manufacturer recommendations for Poly(A) messenger RNA protocol. Libraries were validated and quantified by TapeStation, and an equimolecular pool was made, purified using AMPure XP beads and titrated by PicoGreen. Library pool was sequenced on a NovaSeq 6000 in which clusters were formed and sequenced in a 1 × 100 single-read sequencing run. FastQ files were preprocessed with fastp with default parameters. Preprocessed fastq files were aligned to the GRCm38.p6/mm10 mouse genome using Spliced Transcripts Alignment to a Reference. Read counts were extracted using htseq-count in nonstranded mode. Two-conditions differential expression analysis was performed using DESeq2 (ref1) including DESeq normalization.[19] The significance level was set at an adjusted P value <0.05.[19] Gene set enrichment analysis (GSEA) (ref2) was applied using GSEA to the normalized genes read counts obtained from DESeq2.[19] We used Gene Ontology (Biological Process) Reactome pathways as gene sets. Gene sets with a false discovery rate (FDR) < 0.05 were taken as significant.

Cell culture. C2C12 cells were grown in Dulbecco's modified Eagle's medium (DMEM) enriched with 10% fetal bovine serum and 1% penicillin–streptomycin (growth media, GM). To induce cell differentiation, C2C12 cells at 70% confluence were cultured in DMEM with 2% horse serum (HS) (differentiation media, DM). Cells were preserved in a humidified incubator at 37°C, with an atmosphere of 95% air and 5% CO_2. Media was refreshed every 48 hours.

For collagen content assay, 5×10^4 C2C12 cells were maintained for 24 hours and four days in 12-well plates with GM and DM in the presence and absence of IL-6 (2.5 ng/mL) and dipyridamole (1 μM). The medium was collected, and the cells were fixed with 4% PFA for 20 minutes. Next, cells were washed with PBS

and stained with Sirius Red (0.1%) solution for an hour. After washing the wells with 0.1 M HCl, 0.1 M NaOH was added to release the dye bound to cell collagen and collected for posterior quantification. In parallel, Sirius Red (0.1%) solution was added to cell medium collected for 30 minutes. Next, the medium was centrifuged at 3000 g for six minutes, and cell pellet was collected. Unbound dye was removed by washing the samples with 0.1 M HCl. After centrifugation at 3000 g for six minutes, 0.1 M NaOH was added to release the bound dye, which was collected for quantification. Collagen content in cells and medium was measured with the absorbance at 540-nm wavelength using a microplate reader (Tecan Spark 20M).

Inflammatory study with IL-6 (2.5 ng/mL), IFN-γ (0.1 μg/mL), or lipopolysaccharide (1 μg/mL) in 2% HS for up to four days in the presence or absence of dipyridamole (1 μM) (n = 5) was performed. Briefly, 2 × 10^6 C2C12 cells were seeded in GM for 24 hours. After, inflammatory conditions with dipyridamole were used for 24 hours and four days in DM. At these times, cell lysate was collected in radioimmunoprecipitation assay (RIPA) buffer for Western blot.

A2BR was silenced in C2C12 cells. The 7 × 10^4 C2C12 cells were transfected with Trilencer-27 Fluorescent-labeled transfection control small interfering RNA (siRNA) duplex (1 nM, 5 nM, and 10 nM) using siTran 2.0 siRNA transfection reagents in GM and DM as manufacturer indicates (n = 3 to determine the most effective transfection concentration at 72 hours). Next, different siRNA oligo duplexes (10 nM), targeting *A2BR* and provided by the manufacturer, were tested for gene expressions at 24 and 48 hours and for protein expression at 48 and 72 hours. siRNA duplex pair B (10 nM) was selected for subsequent experiments due to its highest efficiency in silencing both gene and protein expression. siRNA oligo duplex (10 nM) was transfected in three different C2C12 stages: after 24 hours in GM (proliferative state), after 24 hours in DM (premyotube state), and after four days in DM (myotube state). Then, 72 hours after siRNA transfection, C2C12 were treated with or without dipyridamole (1 μM) for another 24 hours. Finally, cell lysate was collected in RIPA buffer for Western blot analysis.

The C2C12 two-dimensional (2-D) monolayer results under inflammatory condition were scaled up to a three-dimensional (3-D) myobundle model. C2C12 myobundles were fabricated following the protocol described by Khodabukus et al.[20] Briefly, molds of polydimethylsiloxane (PDMS) designed for 12-well plates were created from Teflon masters with semicylindrical wells. These molds were sterilized, coated with 0.2% weight/volume Pluronic F-127 to prevent tissue adhesion, and paired with laser-cut Cerex frames (9 × 9 mm^2, 1-mm–wide rim) for myobundle attachment. The frames served as an anchor and guide during hydrogel compaction, ensuring uniaxial cell alignment. C2C12 cells were encapsulated in a hydrogel solution, including bovine fibrinogen, Matrigel, bovine thrombin, and GM following the protocol of Khodabukus et al.[20] The cell and hydrogel mixture was polymerized in the PDMS molds, and myobundles were cultured during four days. Then, the frames with myobundles were suspended in DM in the presence of IL-6 (2.5 ng/mL) on day 0 and dipyridamole (1 μM) on day 0 or 7 after changing to DM for 14 days. DM and treatments are replaced every two days. GM and DM media contained 6-aminocaproic acid to avoid fibrinolysis. Brightfield images were taken on days 7 and 14 to analyze the thickness of the fiber at its midpoint. On day 14, samples were either embedded in OCT for cross-sectioning or paired (two myobundles for N = 1 per condition) to obtain sufficient RNA for isolation using TRIzol. DM on days 7 and 14 were collected for subsequent nucleotide analysis via HPLC. For the histology of OCT samples, 10-μm sections were air-dried and fixed in PFA 4% for one hour. After three wash steps with PBS, sections were blocked with 3% BSA in PBS for one hour. Immunofluorescence staining for phalloidin was performed following the protocol of Khodabukus et al.[20] CSA and minimum of Feret analysis of myobundles was performed with Fiji software. RNA extraction and polymerase chain reaction (PCR) analysis are described below.

Western blot. Frozen GA was crushed using a mortar and a pestle cooled with liquid nitrogen. C2C12 cells and GA samples were lysed with RIPA buffer. GA samples were homogenized in a sonicator. Protein concentration was determined by BCA. Then, 10 μg (cell samples) and 40 μg to 50 μg (tissue samples) of protein was assessed in 6% to 15% sodium dodecyl sulfate–polyacrylamide gel electrophoresis and transferred to a nitrocellulose membrane. Membranes were blocked with 3% BSA in Tris-buffered saline containing 0.1% Tween-20 (TBS-T) and incubated overnight at 4°C with primary antibodies. After washing in TBS-T and incubated with secondary antibodies for one hour, immune complexes were visualized using horseradish peroxidase substrate and acquired with AmerSham Imager 600. Reproving with actin or tubulin was performed for protein loaded Ctrl. Digital densitometry band analysis was performed using Quantity One software, and band intensities were expressed relative to actin or tubulin. Variations in intensity are expressed as a percentage of the Sham group on the same day of sacrifice (in GA) and as a percentage of basal levels (day 0 in IL-6 and Ctrl in siRNA experiments) in C2C12 cells. Data are presented as mean ± SEM and normalized to nondifferentiated Ctrl to minimize interexperimental variability.

RNA isolation and reverse transcriptase–PCR. Total RNA was isolated from crushed frozen GA and myobundles using TRIzol reagent according to the manufacturer's instructions. RNA (1 μg) was reverse transcribed with a High-Capacity cDNA Reverse Transcription Kit (2.5 U/μL), with the next reagents in the same reaction: 1 U/μL RNase inhibitor, 2.5 U/μL Random Hexamers, 5 mM $MgCl_2$, 1× PCR buffer II, and 1 mM deoxynucleoside triphosphate. Relative analysis of gene expression was

performed via real-time reverse transcriptase–PCR on a Step One Plus with PowerUp SYBR Green Master Mix following manufacturer's protocol. The primers listed in Supplementary Table S2 were used. Gene expression levels were calculated with the $\Delta\Delta C_t$ method.

Determination of nucleotide concentration via HPLC. GA were lysed with homemade buffer (1 mM phenylmethylsulphonyl fluoride, 1 mM protease inhibitor cocktail, 1 mM sodium orthovanadate, 1 mM sodium fluoride, and 1 mM β-glycerophosphate in PBS) and EHNA (1 μM) to inhibit the adenosine degradation and cellular uptake. GA samples were homogenized in a sonicator, and supernatant were collected and deproteinized with 4 M perchloric acid and 2 M potassium hydroxide and centrifuged at 13,000 rpm for 10 minutes. Also, myobundles DM collected were treated with EHNA (1 μM) and heat shocked at 95°C and centrifuged at 13,000 rpm for 10 minutes. GA and DM supernatants were stored at –80°C until analyzed. HPLC analysis was performed as previously described.[9] Briefly, inosine, adenosine, AMP, ADP, and ATP concentrations were analyzed via HPLC employing a liquid chromatography with a reversed stage column and a UV detector set at 254 nm. The buffer constituted of 0.1 mol/l KH_2PO_4 (pH 7.5), and 18% acetonitrile was run at 1.5 mL/min for 20 minutes. The compounds were recognized and measured based on the retention time, which were compared to known standards using spectrophotometry for calibration.

Statistical analysis. To ensure adequate statistical power, a power analysis was conducted using the Animal Experimentation Ethics Committee (AEEC) sample size calculator software, based on preliminary data. All experiments were planned to achieve a minimum statistical power of 0.8. Outliers were identified and removed using the robust regression and outlier removal method (Q = 1%). Data normality was assessed using the Kolmogorov-Smirnov test. A P value <0.05 was considered statistically significant. Statistical analyses and visualizations were conducted using GraphPad Prism 7. In the animal model, a one-way analysis of variance (ANOVA) followed by Tukey's post hoc test was used to assess differences between groups, whereas paired *t*-tests were employed to compare differences within the same group across different sacrifice days. For the in vitro analysis of myobundles and C2C12 studies, a one-way ANOVA with Tukey's post hoc test was used between groups, whereas paired *t*-tests were employed to compare differences within the same group across different days with DM in HPLC analysis. Data are presented as mean ± SEM with individual data points. No data were excluded, except for the talus joint histology analysis, as detailed in this section.

RESULTS

Dipyridamole counteracts RA development in K/BxN-induced mice. To study the effect of dipyridamole on RA, we employed the K/BxN animal model. As expected, paw thickness and inflammation peaked 15 days after the injection of K/BxN serum in the RA group and resolved by 28 days. Dipyridamole did not modify paw thickness or inflammation in healthy mice, but it was able to both prevent and treat when it was administered to mice with RA (Figure 1A; Supplementary Figure S1A). The use of antagonists of A2AR or A2BR in mice with RA suppressed dipyridamole anti-inflammatory effect and accelerated the paw's inflammatory process (Supplementary Figure S2A). Histology of the RA ankle at the highest point of inflammation (15 days) (Figure 1B) showed that the talus and tibia bones were in contact due to the expansion and invasion of synovial pannus. Dipyridamole reduced pannus formation and inflammatory infiltrate by reducing the synovitis score in mice with RA as preventive or therapeutic treatment (Figure 1B).

Having shown that dipyridamole reduced paw inflammation and improved synovial tissue in mice with RA, we next examined its effects on systemic inflammation associated with RA. In healthy mice, dipyridamole treatment did not alter systemic proinflammatory or anti-inflammatory cytokines. In mice with RA, an increase of *CRP* (2.05-fold change of Sham) and proinflammatory cytokines such as *IFN-γ* (6.2-fold change of Sham), IL-1β (19.1-fold change of Sham), TNF-α (3.9-fold change of Sham), or IL-6 (3.5-fold change of Sham) were observed on day 15, but dipyridamole treatment reduced their levels. This increase was not observed in mice with RA on day 28. An anti-inflammatory response was activated in mice with RA by increased IL-10 levels (3.2-fold change of Sham) on day 15 and IL-13 (7.2-fold change of Sham) on day 28. Dipyridamole enhanced anti-inflammatory response with IL-5 (2.1-fold change of Sham or 1.6-fold change of RA), IL-9 (2.2-fold change of Sham or 3-fold change of RA). and IL-10 (4.5-fold change of Sham or 1.4-fold change of RA) as preventive treatment or IL-5 (3.5-fold change of Sham or 2.7-fold change of RA), IL-9 (3.1-fold change of Sham or 4.2-fold change of RA), and IL-10 (8-fold change of Sham or 2.5-fold change of RA) as therapeutic treatment in mice with RA on day 15. Therapeutic administration of dipyridamole produced high levels of IL-13 on days 15 (7.3-fold change of Sham or 4.2-fold change of RA) and 28 (12.2-fold change of Sham). MCP-1 levels remained consistently elevated in mice with RA on days 15 (6.9-fold change of Sham) and 28 (4.6-fold change of Sham). Dipyridamole induced a progressive reduction of MCP-1 levels in mice with RA as preventive treatment on days 15 (–1.9-fold change of RA) or 28 (–3-fold change of RA) and as therapeutic treatment on days 15 (–1.4-fold change of RA) or 28 (–2-fold change of RA). In addition, dipyridamole induced vascular endothelial growth factor (VEGF) in Dipy (2.2-fold or 3.2-fold change of Sham on days 15 or 28, respectively), RA + Dipy D0 (1.9-fold or 3.2-fold change

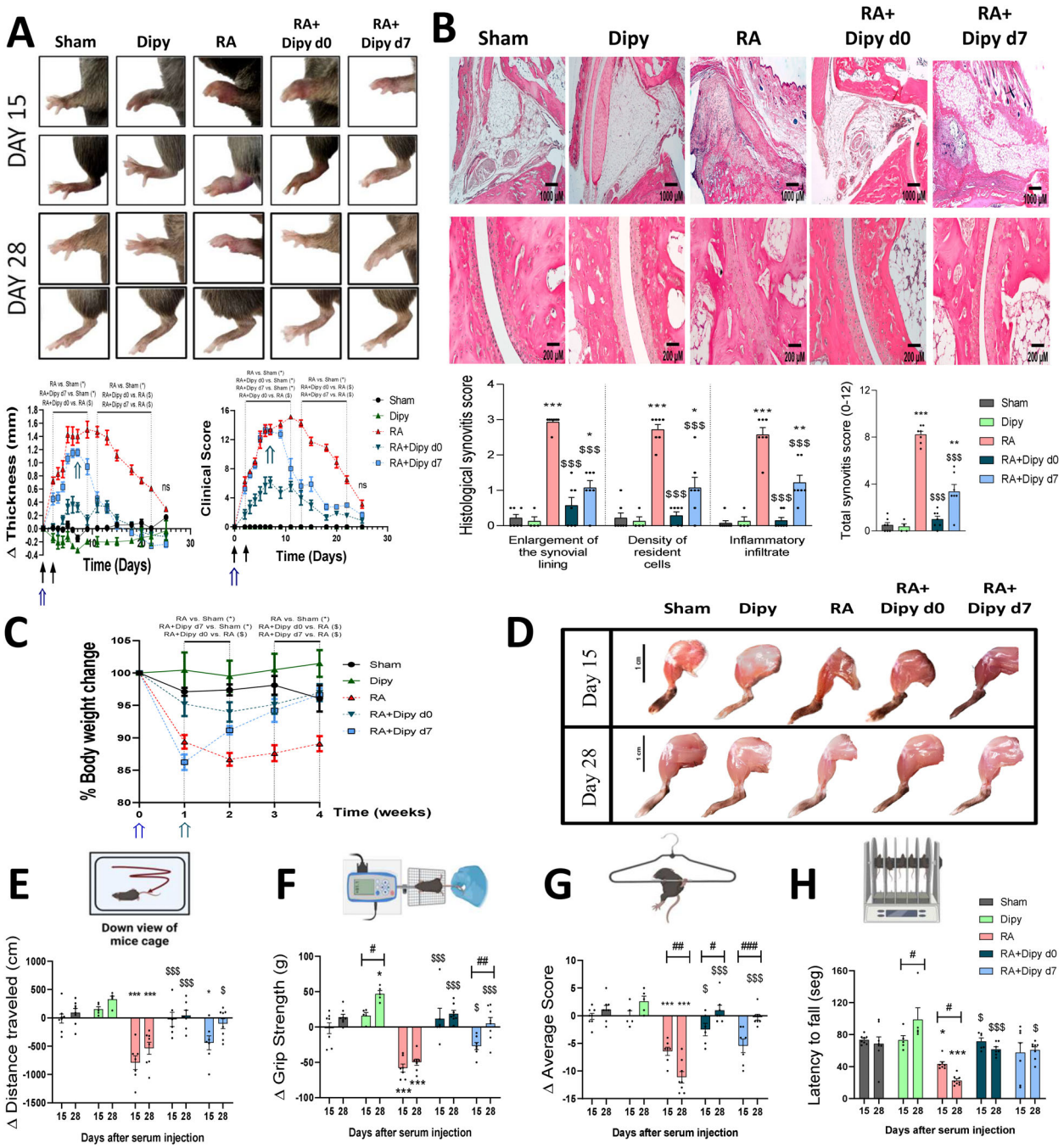

Figure 1. Dipyridamole counteracts pawn inflammation, synovial pannus formation in the talus, body weight loss, and physical activity decline in mice with RA. (A) Macroscopic photographs of thickness and clinical score analysis of hind and fore limbs of mice. (B) Global synovitis score and representative photographs of space between talus and tibia bones on day 15. (C) Body weight changes from day 0 to 28 after K/BxN serum injection. (D) Representative images of hind limb muscles at day of sacrifice. Motor activity tests of (E) ambulatory activity, (F) forelimb grip strength test, (G) two-limb hanging test, and (H) rotarod, represented as difference between the values obtained at days 15 or 28 and before RA induction. Black arrow indicates the days of K/BxN serum administration. Dark and light blue arrows represent the starting days of preventive and therapeutic dipyridamole administration, respectively. Synovial and bone images of the talus joint were acquired at 4× and 20× magnification, respectively. Photographs of the hind and fore limb or hind limb muscles of mice were taken with a mobile device. Analysis of variance followed by Tukey's post hoc test was used to assess differences between groups, whereas paired *t*-tests were employed to compare differences within the same group across different sacrifice days. Differences are represented as follows: *Sham vs other groups at same day; $RA vs RA + Dipy at same day; #between same group and different day. Single symbol represents $P < 0.05$, double symbol represents $P < 0.01$, and triple symbol represents $P < 0.005$. Results are presented as mean ± SEM. N = 5–8 per group for thickness, clinical score, body weight, and physical activity analysis. N = 4–8 per group for synovitis score study. Dipy D0, preventive treatment with dipyridamole from day 0 after rheumatoid arthritis induction; Dipy D7, therapeutic treatment with dipyridamole from day 7 after rheumatoid arthritis induction; RA, rheumatoid arthritis.

of Sham on days 15 or 28, respectively) and RA + Dipy D7 (1.7-fold-change of Sham on day 15) (Supplementary Table S3).

Dipyridamole prevents muscle and bone loss and white adipose tissue gain in mice with RA. Within 28 days, Sham and Dipy mice did not change body weight, whereas mice with RA showed a progressive weight loss. Dipyridamole treatment (both preventive and therapeutic) avoided weight loss in mice with RA (Figure 1C). On day 28 after serum induction, mice with RA showed a sarcopenic phenotype not observed with dipyridamole treatment (Supplementary Figure S1B). Macroscopic hind paw analyzed by digital photography showed an increase of hind limbs muscle size in Dipy mice and a musculature decrease in mice with RA that was recovered with dipyridamole treatment (Figure 1D). The use of A2AR or A2BR antagonists in mice with RA blocked dipyridamole maintenance of body and muscle weight, mimicking the sarcopenic phenotype reported on day 15 in mice with RA. Specifically, the A2BR antagonist further increased body weight loss in mice with RA during the second week (Supplementary Figures S2B and C).

Changes in mice's weight and macroscopic musculature could indicate an alteration in body composition. DXA scanning was performed to analyze body composition changes on day 28 (Supplementary Table S4). Dipy mice showed an increase in lean mass. On the other hand, mice with RA showed a loss of BMD and BMC that were prevented with dipyridamole treatment. Furthermore, lean mass was reduced, whereas fat mass was increased in mice with RA. Dipyridamole counteracted these alterations, maintaining lean mass and fat mass parameters like Sham mice (Supplementary Table S4).

In addition to DXA analysis, tissues were collected during sacrifices. Dipy mice developed an increase of brown adipose tissue (BAT). Mice with RA showed GA, TA, and BAT weight loss, with a gain of white adipose tissue (WAT). Mice with RA treated with dipyridamole prevented this muscle loss and increased BAT with a reduction of WAT. In addition, therapeutic administration of dipyridamole reversed GA weight loss and WAT gain in mice with RA (Supplementary Table S5). The use of A2AR or A2BR antagonists in mice with RA abolished the effect of dipyridamole in restoring BAT and TA loss, further exacerbating GA muscle wasting with A2BR antagonist on day 15 (Supplementary Table S6).

Dipyridamole counteracts muscle activity decline in mice with RA. Physical activity tests were performed to evaluate motor development (Figures 1E–1H). Sham mice did not change their physical performance. Dipy mice improved in strength and motor coordination at 28 days of treatment. Mice with RA exhibited a physical activity decline on day 15, which persisted through 28 days. Preventive treatment with dipyridamole improved ambulatory activity, grip strength, endurance in suspension tests, and motor coordination at 15 days in mice with RA. Therapeutic administration of dipyridamole enhanced the physical performance of mice with RA at 28 days of treatment (Figure 1E). In mice with RA, administration of A2AR or A2BR antagonists inhibited the effect of dipyridamole, sustaining the decline in physical activity on day 15. Notably, treatment with A2BR antagonists further exacerbated the reduction in endurance when suspension tests in mice with RA were performed (Supplementary Figure S2D).

Systemic and muscle inflammation markers in mice with RA are reduced with dipyridamole. Having shown that dipyridamole reduced systemic inflammation and improved physical performance in mice with RA, we next investigated the inflammatory state of the GA muscle (Supplementary Table S7). Dipy mice did not change any proinflammatory or anti-inflammatory cytokine level in GA. On the contrary, RA GA had an increase in proinflammatory cytokines IFN-γ (2.6-fold change of Sham), TNF-α (2.1-fold change of Sham), IL-1α (2.1-fold change of Sham), IL-1β (2.3-fold change of Sham), IL-6 (10.5-fold change of Sham), IL-12 (2.4-fold change of Sham), and CXCL1 (3.7-fold change of Sham) on day 15, being reduced by dipyridamole (not IL-12). RA also induced an increase in IL-4 (2.1-fold change of Sham) and IL-10 (2.4-fold change of Sham) anti-inflammatory cytokines on day 15, enhanced by dipyridamole treatment in IL-10 (3.4-fold or 6.5-fold change of RA for preventive or therapeutic treatment, respectively) and IL-13 (2-fold or 13.3-fold change of Sham for preventive or therapeutic treatment, respectively) (Supplementary Table S7). MCP-1 was increased in mice with RA (8.1-fold or 2.4-fold change of Sham on days 15 or 28, respectively), and dipyridamole prevented this on day 15 (–1.8-fold change of RA) and treated on day 28 (–2-fold change of RA). Dipyridamole induction of systemic VEGF was also observed in muscle on day 28 Dipy (1.7-fold change of Sham), RA + Dipy D0 (1.5-fold change of Sham), and RA + Dipy D7 (1.51-fold change of Sham) mice (Supplementary Table S7).

Cell processes altered in the transcriptome of dipyridamole-treated mice with RA. We compared the transcriptome of mice with RA and RA + D0 mice at 15 days postinduction. Although no significant differences were found at gene level, GSEA extracted a total of 169 Gene Ontology Biological Process and 18 Reactome pathways significantly enriched in dipyridamole-treated mice with RA (FDR < 0.05). Supplementary Figure S2 shows the biologic processes up-regulated in RA + D0 mice. We highlight those related to inflammation processes including T cell–mediated immunity, chronic inflammatory responses, positive regulation of cytokine production, IL-10 production, regulation of neutrophil migration, and chemokines production, among others. We also highlight those related to muscle cell migration, regulation of tissue remodeling, collagen catabolic process, lipid modification, secondary metabolic processes, and bone remodeling and resorption.

Dipyridamole preserves muscle architecture and stimulates the regenerative process of myogenesis in RA. Histologic analysis of TA by H&E, ATPase, and Picrosirius Red staining was performed to evaluate TA physiology. An increase of muscle fiber CSA was reported in dipyridamole mice at 28 days of treatment. On the contrary, mice with RA presented an atrophy of muscle fibers. Preventive treatment with dipyridamole counteracted CSA reduction after 15 days in mice with RA, but therapeutic administration was only effective after 28 days (Figure 2A). Also, fibrosis between TA fibers was observed in mice with RA on days 15 and 28, prevented with dipyridamole treatment. In RA + D7 mice, the TA fibrosis persisted on day 28 (Figure 2B). The reduction of collagen deposits with dipyridamole was reproduced in C2C12 muscle cells under inflammatory conditions (Supplementary Figure S3). When percentage of type I and II fibers was studied in TA by ATPase staining, a decrease of type I fibers in mice with RA was observed, concomitant with an increase in type II fibers at 15 and 28 days after serum induction (Figure 2C). This was counteracted with dipyridamole (Figure 2C).

Administration of either A2AR or A2BR antagonists in mice with RA abrogated the preventive effects of dipyridamole on muscle morphology. Both antagonists prevented the recovery of muscle architecture, leading to persistent muscle fiber atrophy, with a pronounced decrease in CSA particularly evident in the A2BR antagonist–treated group. Moreover, muscle fibrosis remained in mice with RA treated with the A2BR antagonist despite dipyridamole administration, whereas inhibition of A2AR did not impair the antifibrotic effect of dipyridamole. In addition, blockade of either A2AR or A2BR reversed the dipyridamole-induced shift in muscle fiber composition, restoring the predominance of type II fibers characteristic of RA muscle (Supplementary Figure S2E).

Muscle homeostasis and regeneration are dependent on the myogenesis process, conducted by proliferative protein Pax7 and differentiation marker myosin heavy chain (MHC). In Sham and Dipy, GA predominated the differentiation state (Figures 2D and 2E). On the contrary, GA of mice with RA maintained a proliferative state (increased Pax7/MHC ratio) (Figures 2D and 2E). MHC protein expression decreased in mice with RA, and the use of dipyridamole stimulated Pax7 and MHC expression at 15 days and reduced Pax7 expression after 28 days (Figure 2D). This produced a decrease of Pax7/MHC ratio in RA + D0 mice on day 15 and in RA + D7 mice on day 28 (Figure 2E). The administration of A2AR or A2BR antagonists in mice with RA suppressed the dipyridamole-induced increase in MHC expression, maintaining a high Pax7/MHC ratio in GA (Supplementary Figures S2F and S2G).

Dipyridamole stimulates cAMP, AMPK, and creatine kinase via increase of adenosine or AMP levels and A2AR/A2BR activation in mice with RA. Previously, we reported that myogenesis of C2C12 cells was dependent on nucleotide levels.[9] Therefore, we analyzed nucleotide levels in GA extract (Figure 3A). ADP and ATP levels were not modulated. Increment of adenosine and AMP levels with reduction of inosine level was reported in Dipy mice. Mice with RA showed a decrease in adenosine and AMP levels, which were counteracted with dipyridamole after 15 days (Figure 3A). The low levels of adenosine in mice with RA produced a reduction of GA A2AR and A2BR protein expression (Figure 3B), with dipyridamole treatment able to increase A2BR expression in both healthy mice and mice with RA at 15 days. The increase of GA adenosine with dipyridamole, as well as the activation of A2AR and A2BR, suggested that the effect was mediated by cAMP activation. Therefore, we measured cAMP content in GA (Figure 3C). As we previously reported in vitro, dipyridamole induced an increase of cAMP in healthy mice, whereas a decrease in cAMP content was observed in GA of mice with RA. Dipyridamole prevented this on day 15 or reversed it on day 28 in mice with RA (with a trend on day 15). The change in muscle AMP concentration modulated AMP/ATP ratio (Figure 3D), being reduced in mice with RA and recovered with dipyridamole. An increased AMP/ATP ratio activated AMPK in the GA of Dipy mice, whereas the reduced ratio in RA muscle inactivated AMPK. This was counteracted in RA + D0 and RA + D7 mice (Figure 3E). The recovery of AMPK activity by dipyridamole in mice with RA was abolished by the administration of A2AR or A2BR antagonists. Interestingly, inhibition of the A2BR reduced AMPK activity more markedly than A2AR blockade (Supplementary Figure S2H).

Creatine kinase (CK) is described as a key factor that counteracts muscle loss in RA, so CK levels were analyzed in GA of the mice model (Figure 3F).[21] CK protein expression was reduced in RA muscle, and only preventive dipyridamole treatment restored CK levels by day 15. Creatine concentration followed a similar trend (Figure 3G).

Dipyridamole counteracts muscle senescence, atrophy, and necrosis, promoting hypertrophy via myostatin inhibition. Myostatin (MSTN) and insulin-like growth factor (IGF1) are key molecules implicated in the control of muscle hypertrophy. When we measured MSTN expression in GA (Figure 4A), an induction of this marker was reported in mice with RA. In contrast, dipyridamole treatment reduced MSTN levels in mice with RA. The administration of A2AR or A2BR antagonists in mice with RA abolished MSTN reduction observed with dipyridamole. Notably, A2BR suppression increased MSTN expression to a greater extent than observed in mice with RA or in mice with RA treated with the A2AR antagonist (Supplementary Figure S2). No modulation of IGF1 receptor (IGF1R) was found between groups (Figure 4B). On the other hand, dipyridamole in healthy mice induced expression of *mTOR* and *Akt* and avoided the decrease of these markers on day 15 in mice with RA (Figure 4C).

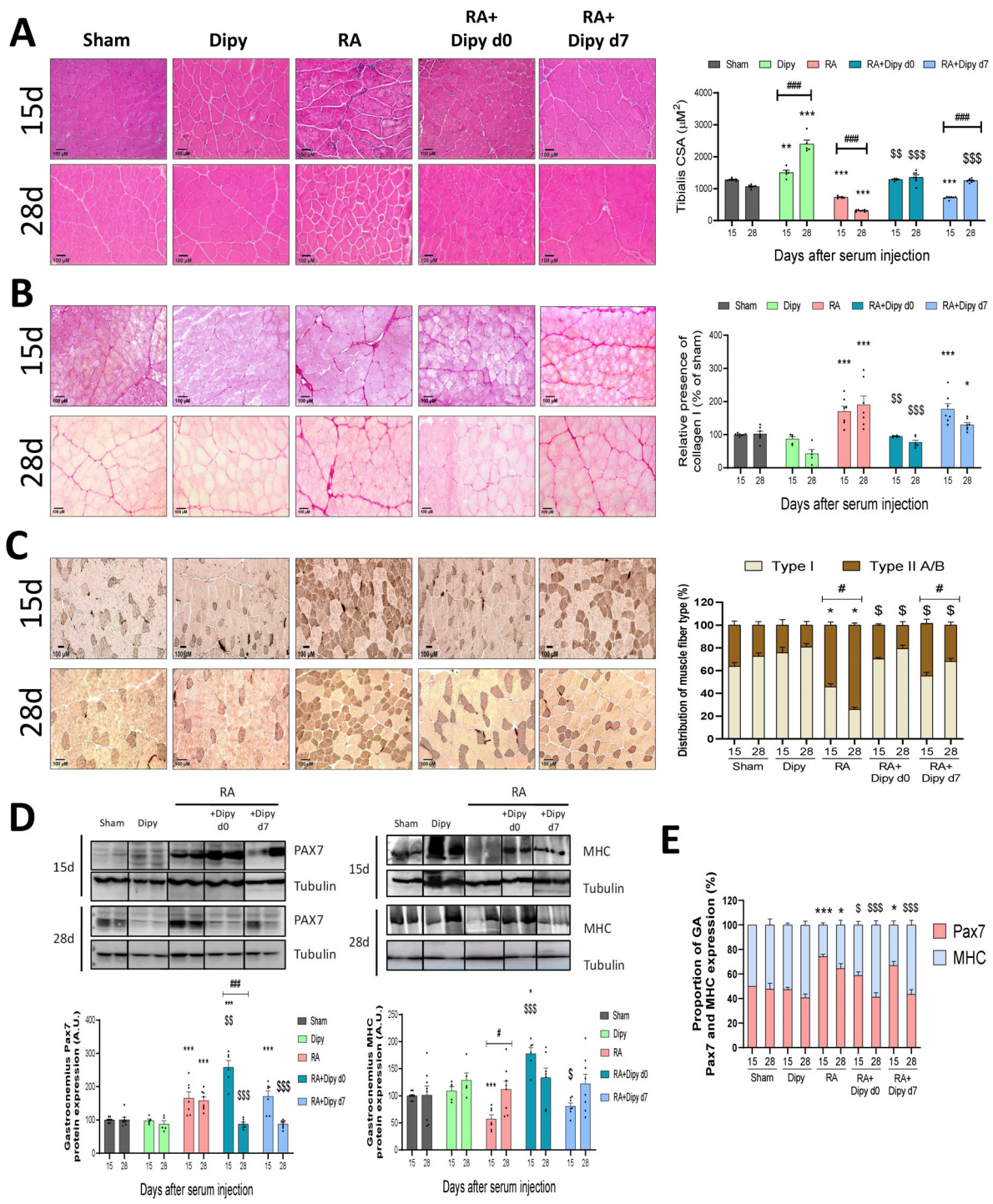

Figure 2. Dipyridamole maintains the muscle architecture, decreases fibrosis, and stimulates the myogenesis in mice with RA. Histology of tibialis anterior analyzed with (A) CSA in hematoxylin and eosin staining, (B) collagen content with Picrosirius Red, and (C) ATPase staining. (D) Western blot of Pax7 and MHC in RA model. (E) GA proportion of Pax7/MHC protein expression. Tibialis anterior images were acquired at 20× magnification. The upper panels show histologic and Western blot analyses at 15 days post–serum induction, whereas the lower panels correspond to 28 days postinduction. Analysis of variance followed by Tukey's post hoc test was used to assess differences between groups, whereas paired *t*-tests were employed to compare differences within the same group across different sacrifice days. Differences are represented as follows: *Sham vs other groups at same day; $RA vs RA + Dipy at same day; #between same group and different day. Single symbol represents $P < 0.05$, double symbol represents $P < 0.01$, and triple symbol represents $P < 0.005$. Results are presented as mean ± SEM. N = 5–8 per group. 15d, 15 days; 28d, 28 days; CSA, cross-sectional area; Dipy D0, preventive treatment with dipyridamole from day 0 after rheumatoid arthritis induction; Dipy D7, therapeutic treatment with dipyridamole from day 7 after rheumatoid arthritis induction; GA, gastrocnemius; MHC, myosin heavy chain; Pax7, paired box 7; RA, rheumatoid arthritis.

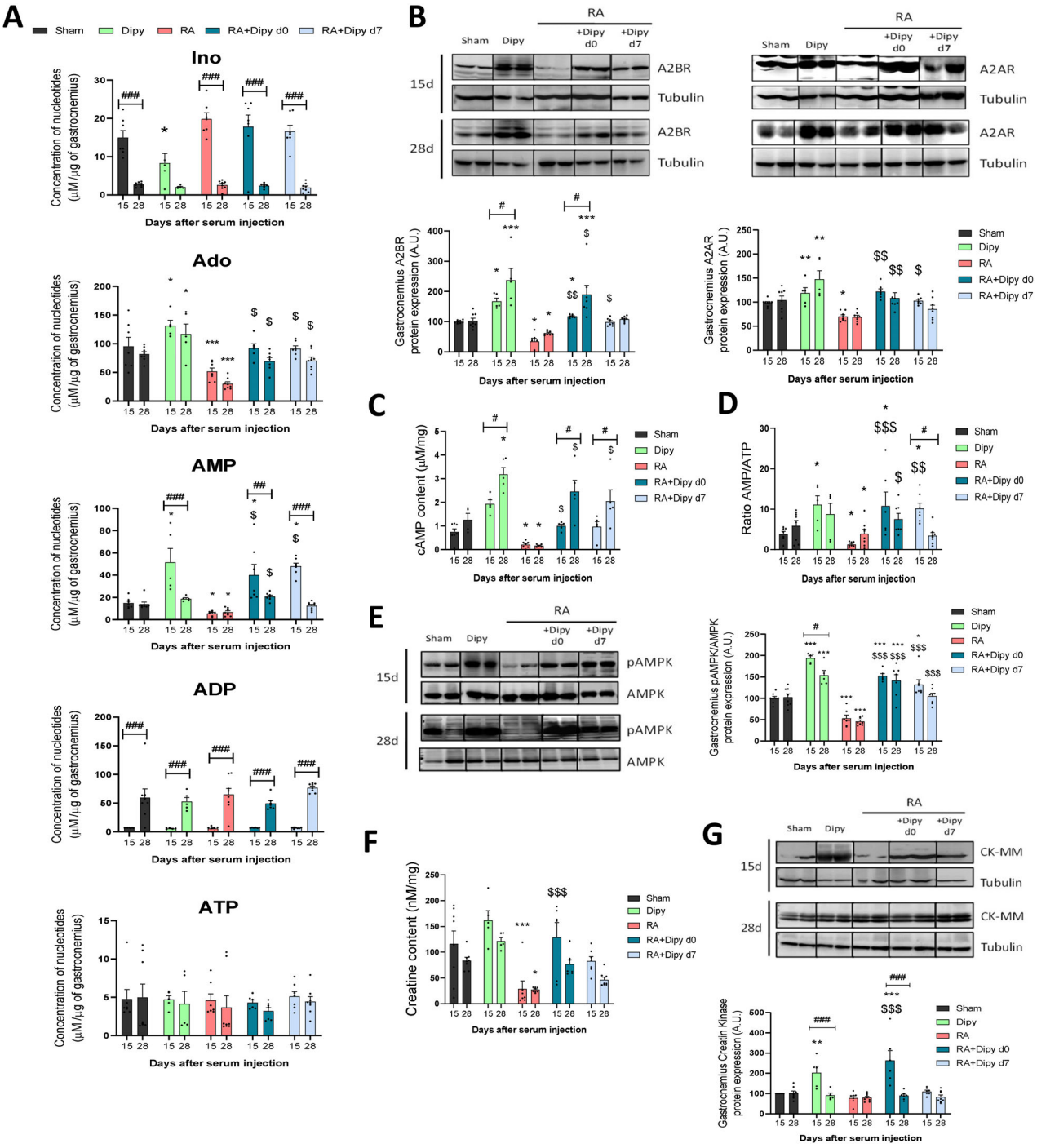

Figure 3. Increment of muscle adenosine and AMP by dipyridamole stimulates cAMP, AMPK, CK, and creatine levels to avoid RA depletion in muscle. (A) Nucleotide content in gastrocnemius of RA model analyzed via high-performance liquid chromatography. (B) Protein expression for A2AR and A2BR studied via Western blot in gastrocnemius. (C) Enzyme-linked immunosorbent assay of cAMP content in gastrocnemius of RA model. (D) Ratio of AMP/ATP in gastrocnemius of mice. (E) Protein expression analyzed by Western blot of pAMPK/AMPK and (F) creatine kinase in gastrocnemius. (G) Enzyme-linked immunosorbent assay of creatine levels in gastrocnemius. The upper panels represent Western blot analyses at 15 days post–serum induction, whereas the lower panels correspond to 28 days postinduction. Analysis of variance followed by Tukey's post hoc test was used to assess differences between groups, whereas paired *t*-tests were employed to compare differences within the same group across different sacrifice days. Differences are represented as follows: *Sham vs other groups at same day; $RA vs RA + Dipy at same day; #between same group and different day. Single symbol represents $P < 0.05$, double symbol represents $P < 0.01$, and triple symbol represents $P < 0.005$. Results are presented as mean ± SEM. N = 5–8 per group. Ado, adenosine; CK-MM, creatine kinase of muscle; Dipy D0, preventive treatment with dipyridamole from day 0 after rheumatoid arthritis induction; Dipy D7, therapeutic treatment with dipyridamole from day 7 after rheumatoid arthritis induction; Ino, inosine; pAMPK, AMP-activated protein kinase phosphorylated; RA, rheumatoid arthritis.

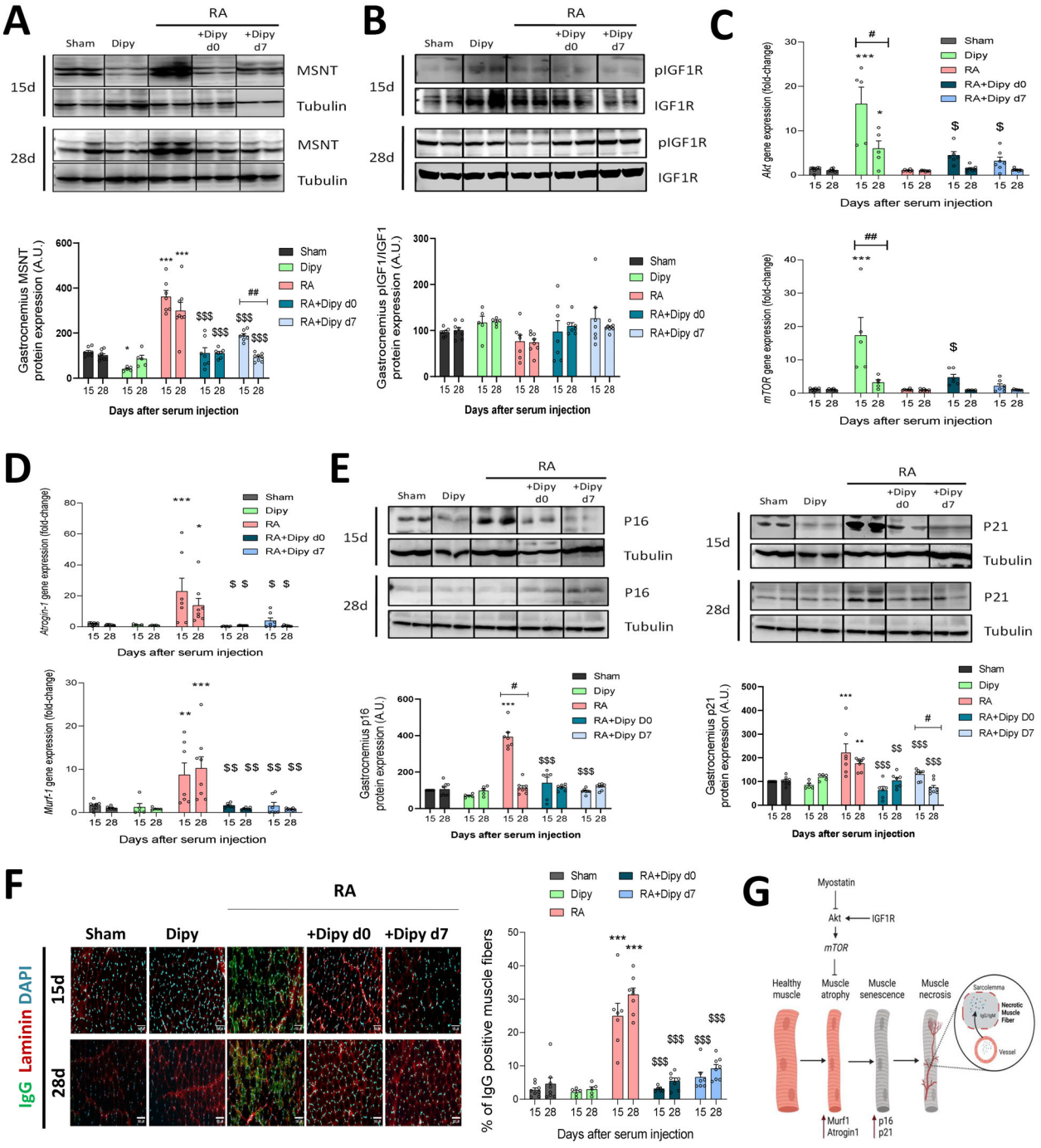

Figure 4. Dipyridamole promotes hypertrophy by down-regulation of MSTN expression and decrease of muscle atrophy, senescence, and progression to necrosis in RA muscle. (A) Western blot of MSTN and (B) pIGF1R/IGF1R in gastrocnemius. (C) Reverse transcriptase–polymerase chain reaction of *Akt* or *mTOR* and (D) atrogenes *Atrogin-1* and *Murf-1* in gastrocnemius. (E) Senescence proteins p16 and p21 studied via Western blot in gastrocnemius. (F) Myonecrosis study via immunofluorescence of IgG infiltration in muscle fibers of tibialis anterior. (G) Graph illustrating of the control of hypertrophy and atrophy, senescence, and necrosis in muscle. The upper panels show immunofluorescence and Western blot analyses at 15 days post–serum induction, whereas the lower panels correspond to 28 days postinduction. Analysis of variance followed by Tukey's post hoc test was used to assess differences between groups, whereas paired *t*-tests were employed to compare differences within the same group across different sacrifice days. Differences are represented as follows: *Sham vs other groups at same day; $RA vs RA + Dipy at same day; #between same group and different day. Single symbol represents $P < 0.05$, double symbol represents $P < 0.01$, and triple symbol represents $P < 0.005$. Results are presented as mean ± SEM. N = 5–8 per group. 15d, 15 days; 28d, 28 days; Dipy D0, preventive treatment with dipyridamole from day 0 after rheumatoid arthritis induction; Dipy D7, therapeutic treatment with dipyridamole from day 7 after rheumatoid arthritis induction; IGF1R, insulin-like growth factor 1 receptor; MSTN, myostatin; mTOR, mechanistic target of rapamycin; pIGF1R, insulin-like growth factor 1 receptor phosphorylated; RA, rheumatoid arthritis.

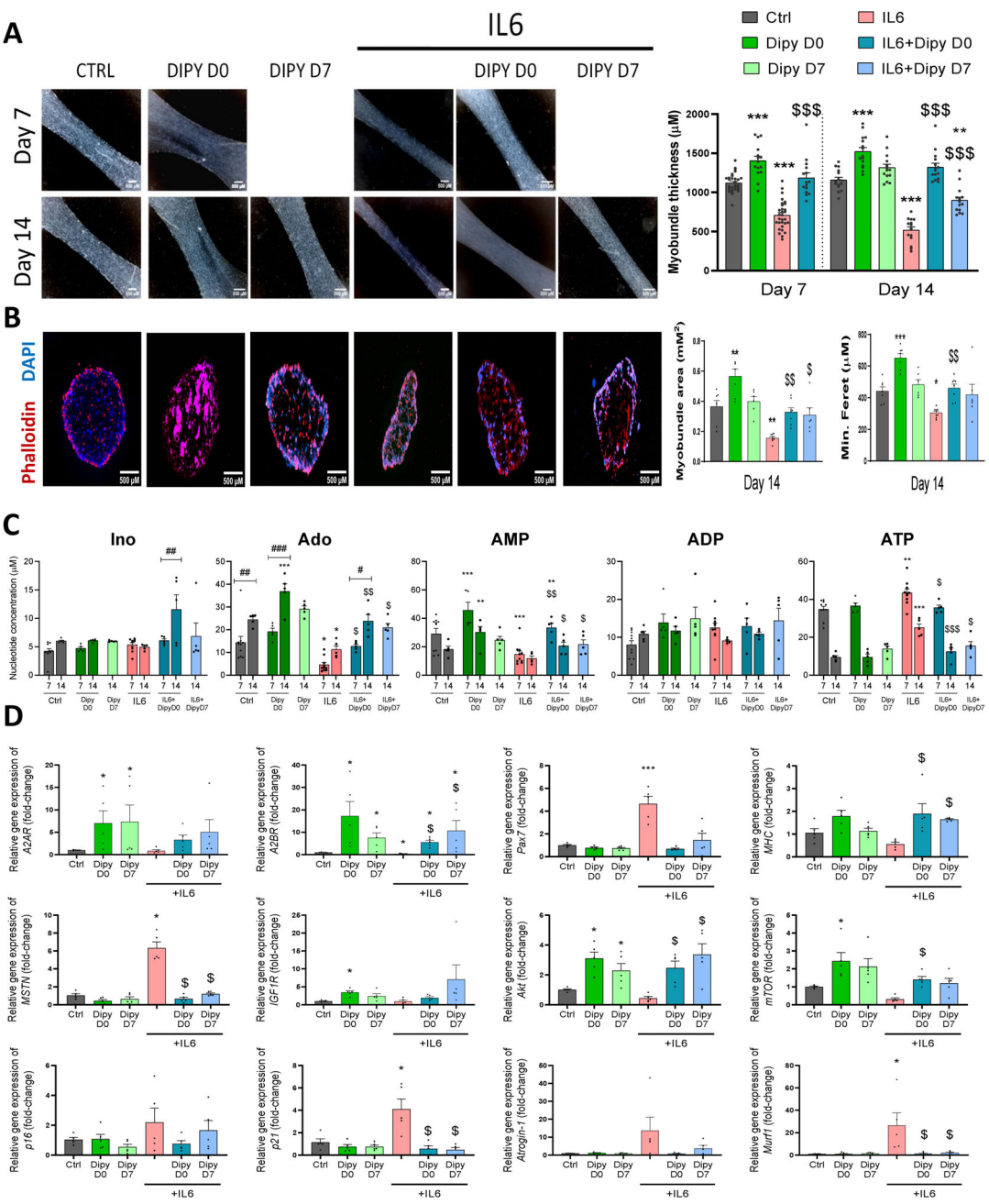

Figure 5. Dipyridamole counteracts muscle atrophy caused by IL-6 as inflammatory condition in three-dimensional myobundle model. (A) Brightfield images and thickness measurements of myobundle models treated with ±IL-6 and ±dipyridamole on days 7 and 14 in differentiation media. (B) Phalloidin and DAPI immunofluorescence staining of myobundle cross-sections on day 14 in differentiation media, with quantification of cross-sectional area and minimum Feret diameter. (C) Nucleotide analysis of supernatant collected on days 7 and 14 in differentiation media via high-performance liquid chromatography. (D) Reverse transcriptase–polymerase chain reaction expression of *A2AR*, *A2BR*, *Pax7*, *MHC*, *MSTN*, *IGF1R*, *Akt*, *mTOR*, *p16*, *p21*, *Atrogin-1*, and *Murf-1* genes in myobundles on day 14 in differentiation media. Brightfield images were taken using 4× magnification. Immunofluorescence images were taken using 10× magnification. Significant differences were assessed using a Kruskal-Wallis test followed by Tukey's post hoc test between groups, whereas paired *t*-tests were employed to compare differences within the same group across different days with differentiation media in high-performance liquid chromatography analysis. Differences are represented as follows: *control vs other groups; $IL-6 vs IL-6 + Dipy; #same group in different days with DM. Single symbol represents $P < 0.05$, double symbol represents $P < 0.01$, and triple symbol represents $P < 0.005$. Results are presented as mean ± SEM. N = 30 of Ctrl and IL-6 groups or N = 15 for other groups at day 7 with differentiation media, and N = 15 for all groups at day 15 with DM in thickness study. Ctrl and IL-6 were divided into two groups with the same sample size after day seven to include Dipy D7 treatment. N = 5 for cross-sectional area, high-performance liquid chromatography, and gene analysis in all groups. Ado, adenosine; Ctrl, control; Dipy D0, preventive treatment with dipyridamole from day 0; Dipy D7, therapeutic treatment with dipyridamole from day 7; IL-6, interleukin-6; Ino, inosine; MHC, myosin heavy chain; MSTN, myostatin; mTOR, mechanistic target of rapamycin; pAMPK, AMP-activated protein kinase phosphorylated; Pax7, paired box 7; pIGF1R, insulin growth factor 1 receptor phosphorylated.

Skeletal muscle atrophy is triggered by the induction of atrogenes. An increase in atrogenes *Atrogin-1* and *Murf-1* was reported in mice with RA, which was prevented and treated by dipyridamole (Figure 4D). Additionally, analysis of muscle senescence markers p21 and p16 was performed (Figure 4E). Both p21 and p16 protein expression were increased on day 15 in mice with RA, and the remaining p21 was elevated on day 28. Dipyridamole was able to decrease both in mice with RA independent of administration protocol (Figure 4E).

To understand if the fiber atrophy and senescence observed in RA muscle progressed to myonecrosis, this process was analyzed in TA. An induction of myonecrosis was observed in mice with RA on day 15, with dipyridamole able to avoid the muscle necrosis (Figure 4F). This model suggests that muscle homeostasis in RA was dependent on muscle hypertrophy to control atrophy and posterior senescence, which progress to necrosis (Figure 4G).

Dipyridamole counteracts IL-6–induced muscle atrophy in a 3-D myobundle model. It is described that the inflammatory environment promotes muscular atrophy.[22] Among the three different inflammatory insults tested herein, IL-6 reflected more similar results to the murine model in the C2C12 monolayer culture (Supplementary Figure S4). Therefore, we have used a 3-D myobundle model treated with IL-6 as an inflammatory condition to confirm the muscle anti-inflammatory and hypertrophic effect of dipyridamole (Figure 5). Our observations indicate that the inflammatory environment induced atrophy of muscle fibers in vitro, with reduced thickness (Figure 5A) and CSA (Figure 5B). On the contrary, dipyridamole induced growth of myobundle after 14 days of treatment. This effect explains that dipyridamole was able to counteract myobundle atrophy in inflammatory conditions (Figure 5B). However, minimum Feret diameter and proper spherical morphology were not restored in IL-6 + Dipy D7 myobundles. Extracellular nucleotide levels were measured on days 7 and 14 of treatments (Figure 5C). IL-6 reduced extracellular adenosine and increased extracellular ATP. Dipyridamole, with or without IL-6, increased extracellular adenosine and AMP after 14 and 7 days of treatment, respectively. Dipyridamole also reduced IL-6–induced extracellular ATP levels. IL-6 stimulated the same pathways as those reported in RA muscle with reduction of *A2BR*, induction of proliferative *Pax7*, and increase of atrophy and senescence genes (Figure 5D). Dipyridamole increased *A2BR* expression, but *A2AR* up-regulation was observed only under non-inflammatory conditions (Figure 5D). In addition, dipyridamole under inflammatory conditions promoted *MHC* expression and avoided atrophy and senescence genes, inhibiting *MSTN*, *p21*, and *Murf-1* expression and stimulating hypertrophic *Akt* gene or *mTOR* but only after 14 days of treatment (Figure 5D).

Depletion of A2BR by siRNA abolishes dipyridamole effect on muscle cells, producing alterations in myogenesis and promoting atrophy in C2C12 cells. In vivo model demonstrated that dipyridamole exerts not only an anti-inflammatory action in mice with RA but also a direct A2BR-dependent hypertrophic effect in muscle of Dipy mice. Accordingly, we aimed to determine the dependence of A2BR for dipyridamole effect in muscle cells under noninflammatory conditions. Therefore, we inhibited A2BR in vitro using siRNA to corroborate the dipyridamole effect in muscle cells. Then, 10 μM siRNA was used after testing the transfection effectiveness on C2C12 cell line (Supplementary Figure S5). As we previously reported, dipyridamole treatment stimulated A2BR, PKAα, pCREB, and pAMPK expression. In all myogenesis stages, the scramble vector did not modulate the proteins analyzed (Figures 6A–6C). The inhibition of A2BR by siRNA was effective in all transfection times, producing a reduction of PKAα, pCREB, and pAMPK expression (Figures 6A–6C). The inhibition of A2BR expression altered the myogenesis process at four days in DM (differentiation medium), maintaining the cells in proliferative state with an increase in Pax7 and a decrease in MHC expression (Figure 6C). No modulations in myogenesis were reported in growth medium (GM) or in DM for 24 hours (Figures 6A and 6B). Furthermore, A2BR silencing produced an increase of MSTN in all states of myogenesis studied (Figures 6A–6C). Dipyridamole treatment after A2BR inhibition by siRNA was ineffective to stimulate A2BR pathway or counteract MSTN increase in all cell states or the myogenic alterations on day four in DM.

DISCUSSION

Beyond joint inflammation, RA is associated with an increased risk of several comorbidities, including alterations in body composition characterized by reduced muscle mass and strength.[1] This study demonstrates that dipyridamole attenuated joint swelling and decreased systemic inflammation. In addition, it improved physical activity and body weight, mitigating muscle inflammation and atrophy in mice with RA. We also found that the improvement in RA muscle was directly mediated by an anabolic mechanism involving downregulation of MSTN expression, which also reduces myogenic alterations, atrophy, senescence, and necrosis. These effects of dipyridamole in RA muscle were related with increased adenosine and AMP levels, which activate A2BR and downstream cAMP/AMPK signaling pathways. We also found that A2BR suppression, which blocked dipyridamole effect, directly correlated with MSTN up-regulation and myogenic alterations in C2C12 cells.

In this study, we demonstrated that both preventive and therapeutic administration of dipyridamole attenuated arthritis severity and systemic inflammation, reduced bone-invasive synovial pannus in the ankle, and lowered systemic levels of CRP, IL-1β, IL-6, TNF-α, IFN-γ, and MCP-1, consistent with findings in

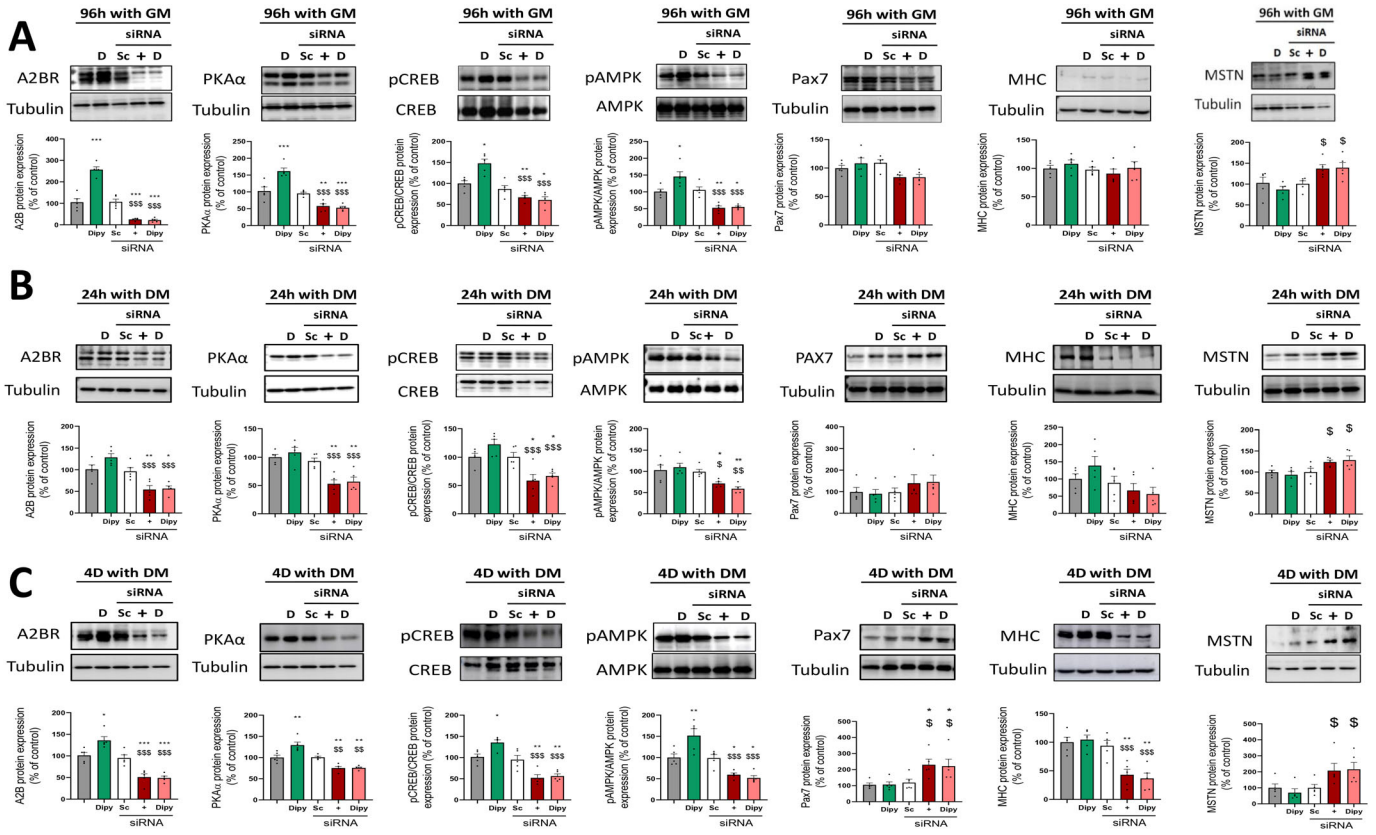

Figure 6. Silencing of A2BR expression inhibits dipyridamole effect in C2C12 cell line, causing myogenesis alterations and increase of MSTN. (A) Protein expression of A2BR, PKAα, pCREB/CREB, MSTN, Pax7, and MHC analyzed via Western blot in C2C12 ± siRNA for A2BR ± dipyridamole at 96 hours with GM, (B) 24 hours in DM, and (C) four days in DM. Significant differences were assessed using a Kruskal-Wallis test followed by Tukey's post hoc test. Differences are represented as follows: *control vs other groups; $siRNA/siRNA+Dipy vs Dipy. Single symbol represents $P < 0.05$, double symbol represents $P < 0.01$, and triple symbol represents $P < 0.005$. Results are presented as mean ± SEM. N = 5 in all conditions. + represents siRNA. 4D, 4 days; 24h, 24 hours; D, dipyridamole; DM, differentiation medium; GM, growth medium; MHC, myosin heavy chain; MSTN, myostatin; pAMPK, AMP-activated protein kinase phosphorylated; Pax7, paired box 7; pCREB, transcription factor cAMP response element-binding protein phosphorylated; PKAα, protein kinase A α subunit; Sc, scramble small interfering RNA; siRNA, small interfering RNA.

patients with RA.[23] Our results address a significant gap because prior evidence on the role of dipyridamole in chronic arthritis is limited.[24] A previous clinical study that used dipyridamole in patients with RA did not report an improvement in disease severity or CRP. However, a small sample size and the subtherapeutic dose of dipyridamole used may have been insufficient to elevate circulating adenosine levels and trigger a robust anti-inflammatory response in patients.[24] Previous studies in rats with AiA showed that therapeutic administration of dipyridamole reduced joint inflammation and pannus formation.[25] In this model, dipyridamole administration for 10 days reduced proinflammatory cytokines and stimulated IL-10 synthesis, replicating the anti-inflammatory effect of MTX.[16] The anti-inflammatory effect of dipyridamole was associated with elevated circulating adenosine levels, which activated the A2AR/A2BR axis and promoted an increase of cAMP.[26,27]

The K/BxN mouse model of RA was used in this study. Although this model produces only anti–glucose-6-phosphoisomerase antibodies and does not fully replicate the autoimmune features of patients with RA, other RA models also fail to reproduce the human RA autoimmunity.[28] Another limitation of the K/BxN model is that it is self-resolving and therefore does not fully recapitulate the chronic, T cell–driven autoimmune pathology and long-term tissue remodeling observed in human RA.[29] Consequently, validation in a chronic RA model is necessary in future studies. It is well established that the K/BxN model develops severe inflammation in the paws.[28] Current treatments, including MTX, dexamethasone, tofacitinib, and bDMARDs, have demonstrated anti-inflammatory effects in this animal model, as evidenced by reduced clinical scores.[30–34] However, these studies offered limited insight into inflammatory cytokine profiles of RA models.[30,32–34] Our study consistently demonstrates that dipyridamole is a pharmacological agent that improves both joint and systemic inflammation in this RA model dependent of A2AR or A2BR stimulation. The robust systemic anti-inflammatory response observed may contribute to reduced inflammation in extra-articular tissues, such as skeletal muscle. Notably, direct anti-inflammatory effects in these tissues were also observed,

suggesting that dipyridamole exerts both systemic and tissue-specific benefits.

Although current RA therapies have improved disease control, they often fail to address associated changes in body composition, especially the loss of muscle mass and strength.[5,6] RA is a multifactorial condition influenced not only by chronic inflammation but also by physical inactivity, metabolic dysregulation, altered anabolic signaling (eg, *IGF-1/Akt/mTOR*), and increased catabolic cytokines such as TNF-α and IL-6. Although anti-inflammatory treatments reduce circulating cytokines, they often fail to restore the anabolic-catabolic balance required for muscle maintenance and regeneration.[3,6] Transcriptomic analyses of RA + Dipy D0 showed that gene expression functions implicated in muscle cell migration and muscle remodeling were also enriched, suggesting that dipyridamole may exert a direct anti-inflammatory–independent effect on skeletal muscle function.[5,6] Additionally, transcriptomic analysis revealed enrichment of T cell apoptosis and cell-mediated immunity functions in RA + Dipy D0 muscle, suggesting its potential applicability to chronic or T cell–mediated models.

An unexpected off-target effect of dipyridamole proved functionally relevant, with Dipy mice exhibiting an anabolic muscle response marked by an increased strength and muscle fiber CSA. This finding suggests that dipyridamole promoted muscle hypertrophy, a mechanism of action that contrasts with conventional RA therapies, which do not produce muscle-anabolic effects.[5,6] We observed that the combined anti-inflammatory and anabolic effects of dipyridamole reversed the reduction in muscle fiber area and mitigated the shift toward oxidative type II fibers in mice with RA. This finding contrasts with previous studies in rabbits with AiA with type I predominance in RA.[31] However, inflammatory myopathies are correlated with a high proportion of type II muscle fibers, corroborating our result in mice with RA.[35] Together with in vitro data (C2C12 monolayer and 3-D myobundle under inflammatory conditions), dipyridamole counteracted the differentiation blockade of muscle cells during both the inflammatory and resolution phases of RA, promoting myofiber formation as observed in healthy muscle. This replicates the condition observed in the atrophic muscle of the hind limb suspension mouse model, characterized by increased satellite cell activation, elevated apoptosis, and enhanced fibrosis.[36] Histologic absence of inflammatory infiltrate in RA muscle fibers at day 15, with dipyridamole treatment, further supports its role in muscle regeneration.[37,38]

Our previous study in muscle cells demonstrated that impaired myogenesis was associated with reduced levels of extracellular adenosine and intracellular AMP.[9] Similar results were obtained in 3-D muscle models under inflammatory conditions for extracellular adenosine. In the RA model, we observed an increase of muscle adenosine and AMP levels with dipyridamole treatment; however, we were unable to differentiate between extracellular and intracellular concentrations. Dipyridamole also produced AMPK activation (via an increased AMP/ATP ratio), cAMP elevation (through adenosine-mediated activation of A2AR and A2BR), and increased CK activity and creatine levels (only with preventive administration), components typically depleted in atrophic muscle.[10,21,39] Notably, A2BR activation and elevated cAMP levels are well-established positive regulators of muscle growth, hypertrophy, and physical activity.[10,40] Although MTX also promotes the increase of extracellular adenosine levels, it activates other adenosine receptors such as A3, which could explain its lack of effect on muscle tissue.[10,41] Conversely, MTX has not been reported to activate A2BR or stimulate the AMPK–cAMP axis, which may explain its lack of effect on sarcopenia despite its well-established anti-inflammatory action. This idea is supported by our previous work, in which exogenous adenosine alone did not reproduce the myogenic effects observed with dipyridamole in muscle cells.[9] Moreover, dipyridamole may enhance extracellular adenosine accumulation more efficiently than MTX, as suggested by studies in patients with RA who are nonresponders to MTX but show disease activity reduction when treated with ticagrelor, another ENT inhibitor similar to dipyridamole.[42] Previous studies have correlated the activation of AMPK or CK and elevated creatine levels with muscle hypertrophy, potentially through the reduction of MSTN expression.[21,43] Muscle MSTN was elevated in mice with RA independent of inflammatory state. This has also been reported in patients with RA, in which MSTN levels did not correlate with CRP or Disease Activity Score in 28 joints scores.[44] It is possible that MSTN decrease observed with dipyridamole in RA muscle was produced by the modulation of adenosine/AMP levels and the activation of cAMP, AMPK, and CK axis and not dependent of anti-inflammatory effect. Mice with RA exhibit a progression from muscle fiber atrophy to senescence and necrosis, a pattern observed in other recognized inflammatory myopathies.[45] This progression was attenuated by dipyridamole treatment. Furthermore, dipyridamole up-regulated hypertrophy-related genes, including *Akt* and *mTOR*, without any changes in *IGF1R* expression. These findings suggest that dipyridamole may stimulate alternative pathways through which these genes are involved, such as those associated with the insulin receptor.[46]

Selective blockade of A2BR in vitro has demonstrated the dependence of A2BR activation on the muscular effects exerted by dipyridamole via PKAα, pCREB, and pAMPK. A2BR depletion altered myogenesis, inducing a proliferative state and increase of MSTN, patterns like those observed in RA mouse muscle, that were not reversed by dipyridamole. These results suggest a correlation between A2BR and hypertrophy in muscle mediated by MSTN. Consistent with these findings, in vivo administration of A2AR or A2BR antagonists in mice with RA suppressed the muscle-protective effects of dipyridamole, maintaining atrophy, the shift toward type II fibers, and the dysregulation of AMPK and MSTN expression. The reduction in AMPK activity and the increase in MSTN levels were more pronounced with A2BR

antagonism, indicating a greater dependence of these pathways on A2BR signaling and a possible heterodimer activity for A2AR and A2BR in muscle.[10]

In addition, we reported collagen catabolic effect of dipyridamole in RA muscle and C2C12 cells under an inflammatory condition with preventive treatment. This effect was not observed in a therapeutic approach because collagen synthesis and degradation are independently regulated processes in skeletal muscle.[47] A2AR stimulation has been linked to increased fibrosis in the skin,[48] suggesting that the muscle fibrosis observed in the therapeutic group may be produced by the absence of collagen degradation in muscle via A2AR activation. Moreover, whereas A2BR blockade preserved muscle fibrosis in mice with RA receiving preventive dipyridamole treatment, A2AR inhibition tended to attenuate it, supporting a potential role of this receptor in collagen deposition and muscle fibrosis.

In our study, CK expression was restored only when dipyridamole was administered preventively but not therapeutically. This timing-dependent effect suggests that once RA-induced muscle atrophy and structural damage are established, the window for metabolic and myogenic recovery may become restricted. CK is a key enzyme in the energy system and is often reduced in atrophic or degenerating muscle fibers.[49] Its lack of recovery with delayed dipyridamole treatment may therefore indicate that the drug's anabolic and metabolic benefits are more effective before irreversible changes, such as fibrosis, necrosis, or satellite cell exhaustion, occur. These findings imply that dipyridamole's ability to restore energy metabolism and promote hypertrophy requires preserved myogenic potential and relatively intact muscle architecture. From a translational perspective, this observation highlights the importance of early intervention in RA-associated myopathy.

Finally, dipyridamole counteracted the increase of WAT observed in mice with RA and promoted BAT content in Sham mice or mice with RA. This browning of adipose tissue depends on A2AR expression, suggesting that dipyridamole, like MTX reported previously, acts through this receptor in adipose tissue.[50–52] This receptor forms a heterodimer with A2BR in BAT to exert its function, explaining why A2BR antagonist suppressed the BAT increase in mice with RA.[10] These results suggest that dipyridamole could activate the same receptors for browning as in muscle. This hypothesis will be further corroborated in future studies. Overall, these findings support the idea that the specific adenosine receptor subtype activated depends not only on the amount of extracellular adenosine generated but also on the mechanism by which each drug increases adenosine levels and the tissue-specific context in which this occurs.

In conclusion, our findings demonstrate that dipyridamole is an effective preventive and therapeutic strategy for joint inflammation in RA, exerting a potent systemic anti-inflammatory effect with additional benefits on skeletal muscle and other affected tissues via A2AR and A2BR activation. In mice with RA, dipyridamole enhanced both muscle mass and function, promoting an anabolic response characterized by MSTN downregulation. These effects were associated with elevated adenosine and AMP muscle levels, activating A2BR receptor and downstream cAMP/AMPK signaling pathways. Similar anabolic effects were observed in healthy animals and in vitro models, suggesting that dipyridamole stimulates muscle beyond its anti-inflammatory action. This direct action on muscle may distinguish dipyridamole from current therapies and holds promise for addressing sarcopenic comorbidities in RA. However, the inability to obtain human muscle samples from patients with RA constitutes a limitation of the present study. Moreover, the anti-inflammatory and muscle-anabolic effects of dipyridamole were demonstrated in the K/BxN model, and these results may not automatically generalize to chronic, T cell–dependent disease. Future research will address these gaps by incorporating human muscle tissue and additional RA models to validate and extend these findings.

ACKNOWLEDGMENTS

Artificial intelligence tools were employed exclusively for language editing, but no generative functions were used in the preparation of this manuscript.

AUTHOR CONTRIBUTIONS

All authors contributed to at least one of the following manuscript preparation roles: conceptualization AND/OR methodology, software, investigation, formal analysis, data curation, visualization, and validation AND drafting or reviewing/editing the final draft. As corresponding author, Dr Mediero confirms that all authors have provided the final approval of the version to be published, and takes responsibility for the affirmations regarding article submission (eg, not under consideration by another journal), the integrity of the data presented, and the statements regarding compliance with institutional review board/Declaration of Helsinki requirements.

REFERENCES

1. Moschou D, Krikelis M, Georgakopoulos C, et al. Sarcopenia in rheumatoid arthritis. A narrative review. J Frailty Sarcopenia Falls 2023; 8(1):44–52. doi:https://doi.org/10.22540/JFSF-08-044
2. Little RD, Prieto-Potin I, Pérez-Baos S, et al. Compensatory anabolic signaling in the sarcopenia of experimental chronic arthritis. Sci Rep 2017;7(1):6311. doi:https://doi.org/10.1038/s41598-017-06581-6
3. Torii M, Itaya T, Minamino H, et al. Management of sarcopenia in patients with rheumatoid arthritis. Mod Rheumatol 2023;33(3):435–440. doi:https://doi.org/10.1093/mr/roac095
4. Day J, Louis C, Swiderski K, et al. Periarticular myositis and muscle fibrosis are cytokine-dependent complications of inflammatory arthritis. JCI Insight 2025;10(7):e179928. doi:https://doi.org/10.1172/jci.insight.179928
5. Teixeira VON, Bartikoski BJ, do Espirito Santo RC, et al. The role of proteasome in muscle wasting of experimental arthritis. Adv Rheumatol 2023;63(1):14. doi:https://doi.org/10.1186/s42358-023-00292-5
6. Hein TR, Peterson L, Bartikoski BJ, et al. The effect of disease-modifying anti-rheumatic drugs on skeletal muscle mass in rheumatoid arthritis patients: a systematic review with meta-analysis. Arthritis

Res Ther 2022;24(1):171. doi:https://doi.org/10.1186/s13075-022-02858-y

7. Webster JM, Kempen LJAP, Hardy RS, et al. Inflammation and skeletal muscle wasting during cachexia. Front Physiol 2020;11:597675. doi:https://doi.org/10.3389/fphys.2020.597675
8. Fredholm BB. Adenosine, an endogenous distress signal, modulates tissue damage and repair. Cell Death Differ 2007;14(7):1315–1323. doi:https://doi.org/10.1038/sj.cdd.4402132
9. Marco-Bonilla M, Herencia R, Fresnadillo M, et al. Dipyridamole activates adenosine A2B receptor and AMPK/cAMP signaling and promotes myogenic differentiation of myoblastic C2C12 cells. Front Pharmacol 2023;14:1247664. doi:https://doi.org/10.3389/fphar.2023.1247664
10. Gnad T, Navarro G, Lahesmaa M, et al. Adenosine/A2B receptor signaling ameliorates the effects of aging and counteracts obesity. Cell Metab 2020;32(1):56–70.e7. doi:https://doi.org/10.1016/j.cmet.2020.06.006
11. Liu YW, Yang T, Zhao L, et al. Activation of Adenosine 2A receptor inhibits neutrophil apoptosis in an autophagy-dependent manner in mice with systemic inflammatory response syndrome. Sci Rep 2016;6(1):33614. doi:https://doi.org/10.1038/srep33614
12. Németh ZH, Lutz CS, Csóka B, et al. Adenosine augments IL-10 production by macrophages through an A2B receptor-mediated post-transcriptional mechanism. J Immunol 2005;175(12):8260–8270. doi:https://doi.org/10.4049/jimmunol.175.12.8260
13. Conesa-Buendía FM, Llamas-Granda P, Larrañaga-Vera A, et al. Tenofovir causes bone loss via decreased bone formation and increased bone resorption, which can be counteracted by dipyridamole in mice. J Bone Miner Res 2019;34(5):923–938. doi:https://doi.org/10.1002/jbmr.3665
14. Cronstein BN, Aune TM. Methotrexate and its mechanisms of action in inflammatory arthritis. Nat Rev Rheumatol 2020;16(3):145–154. doi:https://doi.org/10.1038/s41584-020-0373-9
15. Ward JL, Sherali A, Mo ZP, et al. Kinetic and pharmacological properties of cloned human equilibrative nucleoside transporters, ENT1 and ENT2, stably expressed in nucleoside transporter-deficient PK15 cells. Ent2 exhibits a low affinity for guanosine and cytidine but a high affinity for inosine. J Biol Chem 2000;275(12):8375–8381. doi:https://doi.org/10.1074/jbc.275.12.8375
16. Babu LN, Tyagi MG. Evaluation of the anti-inflammatory effect of dipyridamole, ATP per se and in combination with methotrexate in Freund's adjuvant induced arthritis in rats. Recent Res Science Technol 2010;2(3):71–75.
17. Aartsma-Rus A, van Putten M. Assessing functional performance in the mdx mouse model. J Vis Exp 2014;51303(85):51303. doi:https://doi.org/10.3791/51303-v
18. Krenn V, Morawietz L, Burmester GR, et al. Synovitis score: discrimination between chronic low-grade and high-grade synovitis. Histopathology 2006;49(4):358–364. doi:https://doi.org/10.1111/j.1365-2559.2006.02508.x
19. Love MI, Huber W, Anders S. Moderated estimation of fold change and dispersion for RNA-seq data with DESeq2. Genome Biol 2014;15(12):550. doi:https://doi.org/10.1186/s13059-014-0550-8
20. Khodabukus A, Madden L, Prabhu NK, et al. Electrical stimulation increases hypertrophy and metabolic flux in tissue-engineered human skeletal muscle. Biomaterials 2019;198:259–269. doi:https://doi.org/10.1016/j.biomaterials.2018.08.058
21. van de Velde NM, Koeks Z, Signorelli M, et al. Longitudinal assessment of creatine kinase, creatine/creatinine$_{ratio}$, and myostatin as monitoring biomarkers in Becker muscular dystrophy. Neurology 2023;100(9):e975–e984. doi:https://doi.org/10.1212/WNL.0000000000201609
22. Costamagna D, Costelli P, Sampaolesi M, et al. Role of inflammation in muscle homeostasis and myogenesis. Mediators Inflamm 2015;2015(1):805172. doi:https://doi.org/10.1155/2015/805172
23. Jia Y, Feng B, Ji X, et al. Complement factor H attenuates TNF-α-induced inflammation by upregulating EIF3C in rheumatoid arthritis. J Transl Med 2023;21(1):846. doi:https://doi.org/10.1186/s12967-023-04730-2
24. Forrest CM, Stoy N, Stone TW, et al. Adenosine and cytokine levels following treatment of rheumatoid arthritis with dipyridamole. Rheumatol Int 2006;27(1):11–17. doi:https://doi.org/10.1007/s00296-006-0212-6
25. Gomaa A, Elshenawy M, Afifi N, et al. Influence of dipyridamole and its combination with NO donor or NO synthase inhibitor on adjuvant arthritis. Int Immunopharmacol 2010;10(11):1406–1414. doi:https://doi.org/10.1016/j.intimp.2010.08.006
26. Ramakers BP, Riksen NP, Stal TH, et al. Dipyridamole augments the antiinflammatory response during human endotoxemia. Crit Care 2011;15(6):R289. doi:https://doi.org/10.1186/cc10576
27. Zimmermann GR, Avery W, Finelli AL, et al. Selective amplification of glucocorticoid anti-inflammatory activity through synergistic multi-target action of a combination drug. Arthritis Res Ther 2009;11(1):R12. doi:https://doi.org/10.1186/ar2602
28. Marco-Bonilla M, Fresnadillo M, de la Riva-Bueno M, et al. Animal models in rheumatoid arthritis: is there a correlation between autoantibodies in human pathology and animal models? Biology (Basel) 2025;14(5):460. doi:https://doi.org/10.3390/biology14050460
29. Christensen AD, Haase C, Cook AD, et al. K/BxN serum-transfer arthritis as a model for human inflammatory arthritis. Front Immunol 2016;7:213. doi:https://doi.org/10.3389/fimmu.2016.00213
30. Quan L, Zhang Y, Dusad A, et al. The evaluation of the therapeutic efficacy and side effects of a macromolecular dexamethasone prodrug in the collagen-induced arthritis mouse model. Pharm Res 2016;33(1):186–193. doi:https://doi.org/10.1007/s11095-015-1776-1
31. Bermejo-Álvarez I, Pérez-Baos S, Gratal P, et al. Effects of tofacitinib on muscle remodeling in experimental rheumatoid sarcopenia. Int J Mol Sci 2023;24(17):13181. doi:https://doi.org/10.3390/ijms241713181
32. Gao J, Miao J, Sun H, et al. TNF-α inhibitor ameliorates immune-related arthritis and pneumonitis in humanized mice. Front Immunol 2022;13:955812. doi:https://doi.org/10.3389/fimmu.2022.955812
33. Park JS, Lee D, Yang S, et al. Methotrexate-loaded nanoparticles ameliorate experimental model of autoimmune arthritis by regulating the balance of interleukin-17-producing T cells and regulatory T cells. J Transl Med 2022;20(1):85. doi:https://doi.org/10.1186/s12967-022-03267-0
34. Pérez-Baos S, Gratal P, Barrasa JI, et al. Inhibition of pSTAT1 by tofacitinib accounts for the early improvement of experimental chronic synovitis. J Inflamm (Lond) 2019;16(1):2. doi:https://doi.org/10.1186/s12950-019-0206-2
35. Loell I, Helmers SB, Dastmalchi M, et al. Higher proportion of fast-twitch (type II) muscle fibres in idiopathic inflammatory myopathies - evident in chronic but not in untreated newly diagnosed patients. Clin Physiol Funct Imaging 2011;31(1):18–25. doi:https://doi.org/10.1111/j.1475-097X.2010.00973.x
36. Ferreira R, Neuparth MJ, Ascensão A, et al. Skeletal muscle atrophy increases cell proliferation in mice gastrocnemius during the first week of hindlimb suspension. Eur J Appl Physiol 2006;97(3):340–346. doi:https://doi.org/10.1007/s00421-006-0197-6
37. Mahdy MAA. Skeletal muscle fibrosis: an overview. Cell Tissue Res 2019;375(3):575–588. doi:https://doi.org/10.1007/s00441-018-2955-2
38. Tatsumi R. Mechano-biology of skeletal muscle hypertrophy and regeneration: possible mechanism of stretch-induced activation of

resident myogenic stem cells. Anim Sci J 2010;81(1):11–20. doi:https://doi.org/10.1111/j.1740-0929.2009.00712.x

39. Thomson DM. The role of AMPK in the regulation of skeletal muscle size, hypertrophy, and regeneration. Int J Mol Sci 2018;19(10):3125. doi:https://doi.org/10.3390/ijms19103125
40. Wang Z, Zhang L, Liang Y, et al. Cyclic AMP mimics the anti-ageing effects of calorie restriction by up-regulating sirtuin. Sci Rep 2015;5(1):12012. doi:https://doi.org/10.1038/srep12012
41. Cronstein BN, Sitkovsky M. Adenosine and adenosine receptors in the pathogenesis and treatment of rheumatic diseases. Nat Rev Rheumatol 2017;13(1):41–51. doi:https://doi.org/10.1038/nrrheum.2016.178
42. Garshick MS, Rosenthal PB, Luttrell-Williams E, et al. Ticagrelor added to methotrexate improves rheumatoid arthritis disease severity. Rheumatology (Oxford) 2021;60(11):5473–5475. doi:https://doi.org/10.1093/rheumatology/keab481
43. Das AK, Yang QY, Fu X, et al. AMP-activated protein kinase stimulates myostatin expression in C2C12 cells. Biochem Biophys Res Commun 2012;427(1):36–40. doi:https://doi.org/10.1016/j.bbrc.2012.08.138
44. Lin JZ, Ma JD, Yang LJ, et al. Myokine myostatin is a novel predictor of one-year radiographic progression in patients with rheumatoid arthritis: a prospective cohort study. Front Immunol 2022;13:1005161. doi:https://doi.org/10.3389/fimmu.2022.1005161
45. Kamiya M, Kimura N, Umezawa N, et al. Muscle fiber necroptosis in pathophysiology of idiopathic inflammatory myopathies and its potential as target of novel treatment strategy. Front Immunol 2023;14:1191815. doi:https://doi.org/10.3389/fimmu.2023.1191815
46. Yoon MS. mTOR as a key regulator in maintaining skeletal muscle mass. Front Physiol 2017;8:788. doi:https://doi.org/10.3389/fphys.2017.00788
47. Chen WJ, Lin IH, Lee CW, et al. Aged skeletal muscle retains the ability to remodel extracellular matrix for degradation of collagen deposition after muscle injury. Int J Mol Sci 2021;22(4):2123. doi:https://doi.org/10.3390/ijms22042123
48. Perez-Aso M, Fernandez P, Mediero A, et al. Adenosine 2A receptor promotes collagen production by human fibroblasts via pathways involving cyclic AMP and AKT but independent of Smad2/3. FASEB J 2014;28(2):802–812. doi:https://doi.org/10.1096/fj.13-241646
49. Stucki G, Brühlmann P, Stoll T, et al. Low serum creatine kinase activity is associated with muscle weakness in patients with rheumatoid arthritis. J Rheumatol 1996;23(4):603–608.
50. Verma N, Perie L, Corciulo C, et al. Browning of adipose tissue and increased thermogenesis induced by methotrexate. FASEB Bioadv 2021;3(11):877–887. doi:https://doi.org/10.1096/fba.2021-00058
51. Verma N, Perie L, Silvestro M, et al. Metabolic dysfunction in mice with adipocyte-specific ablation of the adenosine A2A receptor. J Biol Chem 2025;301(2):108206. doi:https://doi.org/10.1016/j.jbc.2025.108206
52. Gnad T, Scheibler S, von Kügelgen I, et al. Adenosine activates brown adipose tissue and recruits beige adipocytes via A2A receptors. Nature 2014;516(7531):395–399. doi:https://doi.org/10.1038/nature13816